

*Republic of Iraq
Ministry of Higher Education and
Scientific Research
University of Baghdad
College of Education for Pure Science
Ibn-AL-Haitham*



The effect of (In₂O₃) on the electrical properties of (ZnO) – based varistor

A Thesis

*Submitted to University of Baghdad / College of Education for Pure Science
(Ibn-AL-Haitham) in partial Fulfillment of the Requirements for the Degree
of Master of Science in Physics*

By

Mustafa Qassim Abbass

Supervisor

Asst. Prof. Dr. Aysar. J. Ibraheem

2019 A.D

1441 A.H

بِسْمِ اللَّهِ الرَّحْمَنِ الرَّحِيمِ


((اللَّهُ نُورُ السَّمَوَاتِ وَالْأَرْضِ مِثْلُ نُورِهِ كَمِشْكَاةٍ فِيهَا
مِصْبَاحٌ الْمِصْبَاحُ فِي زُجَاجَةٍ الزُّجَاجَةُ كَأَنَّهَا كَوْكَبٌ دُرِّيٌّ
يُوقَدُ مِنْ شَجَرَةٍ مَبَارَكَةٍ زَيْتُونَةٍ لَشَرْقِيَةٍ وَلَا غَرْبِيَةٍ يَكَادُ زَيْتُهَا
يَضِيءُ وَلَوْ لَمْ تَمْسَسْهُ نَارٌ نُورٌ عَلَى نُورٍ يَهْدِي اللَّهُ لِنُورِهِ مَنْ
يَشَاءُ وَيَضْرِبُ اللَّهُ الْأَمْثَالَ لِلنَّاسِ وَاللَّهُ بِكُلِّ شَيْءٍ عَلِيمٌ))

صدق الله العظيم

سورة النور آية ﴿ 35 ﴾

Supervisor Certification

I certify that this thesis entitled “(The effect of (In_2O_3) on the electrical properties of (ZnO) - based Varistor)” was prepared by **Mustafa Qassim Abbass**, under my supervision at Physics Department, College of Education for Pure Science Ibn - Al-Haitham University of Baghdad as partial requirement for the degree of Master of Science in Physics.

Signature: 

Name: Dr. Aysar. J. Ibraheem

Title: Assistant Professor

Address: Collage of Education for
Pure Science Ibn - Al - Haitham
University of Baghdad

Date: 11 / 10 / 2019

In view of the available recommendation, I forward this thesis for debate by the examination committee.

Signature: S. A. MAKI

Name: Dr. Samir Ata. Maki

Title: Professor

Address: Collage of Education for
Pure Science Ibn-Al-Haitham
University of Baghdad

Date: 11 / 10 / 2019

Committee Certificate

This is to certify that we have read this thesis entitled (The effect of (In_2O_3) on the electrical properties of (ZnO) - based Varistor), and as an examining committee, examined the student (Mustafa Qassim Abbass) in its content and in our opinion, it is adequate for partial fulfillment of the requirement for the Degree of Master of Science in Physics.

Signature:

Name: Dr. Zainab Abdul Salam Jaber

Al-Ramadhan

Title: Professor

Address: Al-Mustansyriah University

Date: 12 / 12 / 2019

Chairman

Signature:

Name: Dr. Abbas Karim Saadon

Title: Assistant Professor

Address: University of Baghdad

Date: 11 / 12 / 2019

Member

Signature:

Name: Dr. Ridha H. Risan

Title: Instructor

Address: University of Baghdad

Date: 11 / 12 / 2019

Member

Signature:

Name: Dr. Aysar J. Ibraheem

Title: Assistant Professor

Address: University of Baghdad

Date: 11 / 12 / 2019

Member- Supervisor

Approved by the of the College of Education for pure science
Ibn- Al- Haitham, University of Baghdad.

Signature:

Assist. Prof. Dr. Firas Abdulhameed Abdullatif

Behalf/ The Dean of College of Education for pure science/ Ibn Al- Haitham.

Date: 17 / 12 / 2019

Dedication

To my teacher and inspirer, Prophet Muhammad, peace be upon him, to my father and mother who raised me and tired in order to reach the highest degree of science, to my wife who supported me and my children Ahmed and Malak

Mustafa

ACKNOWLEDGMENTS

All praise too Allah his majesty who enabled me to overcome all the difficulties I faced in this study until putting the thesis in its final form.

I would like to thank my supervisor Dr. Aysar. J. Ibraheem for her inspiration and valuable suggestions throughout this research.

A special thanks to Dr. Adel Ismail for his invaluable comments, limitless help and moral support.

I would also like to express my gratitude to the professors and all the staff members of the Department of Physics / Education College for Pure Science / Ibn Al-Haitham.

A great gratitude and thanks go to all my friends and colleagues for always being there for me and continuously supporting me.

Finally, I can never thank my family enough for their love, support and fundamental trust in me.

Abstract

A varistor is a device made of ceramic material. It is used as a protection component in many areas of life. In order to prepare the varistor, the traditional method of ceramic industries is used (solid-state reaction).

XRD tests for zinc oxide powder and Indium oxide nano powder are conducted to determine the degree of purity. After the weighting process, the powders were mixed with water by a magnetic mixer and then dried for 24h. After that, the gases, moisture and some of the impurities are disposed of by burning for 2h at (500°C). Then grinding is carried out, and the samples are compressed in tablets of a radius of 8mm. The samples are placed in the furnace for sintering at three different temperatures of (1000, 1050 and 1100) °C to obtain the required shapes.

XRD examinations are carried out for sintered samples and shows the emergence of several phases which is led by the phase of basic zinc oxide. The crystallite size and the grain size of the samples were measured using the Debay-Shearer equation and images of the scanning electron microscopy (SEM). It turns out that the grain size decreases by increasing the concentrations of (In₂O₃) nano powder and increases with the increase of the sintering temperature.

Because the effect of the breakdown voltage on the grain size, it will increase by increasing the concentration of the indium oxide nano powder. The behavior of the non-linear coefficient (α) can be seen between current and voltage values. It is found that the nonlinear coefficient increased with increasing concentrations of (In₂O₃) nano powder and other oxides. The decrease of (α) with the increase of sintering temperatures is due to the effect of Schottky-barriers between grain boundaries. Furthermore, at higher temperature, the leakage current was decreased when increasing the In₂O₃ concentrations.

The values of the dielectric constant were reduced by increasing the frequency and the high dielectric constant is observed as the sintering temperatures increases. However, the results of the loss factor decreases with increasing In_2O_3 concentrations.

The effect of light and darkness on the properties (current-voltage) of the samples was examined after the light intensity was shed on them as well as in opacity. It is revealed that the electrical properties of the samples are not affected by both tests, which allow us to benefit from the use of varistor in external environmental conditions, especially the effect of sunlight.

CONTENTS

| No. | Subject | Page |
|------------|---|-------------|
| | CHAPTER ONE INTRODUCTION | |
| 1.1 | Introduction | 1 |
| 1.2 | ZnO varistor composition | 2 |
| 1.3 | Some of the varistor electric properties | 3 |
| 1.3.1 | Leakage current (I_L) | 3 |
| 1.3.2 | Break down voltage (Varistor voltage) | 4 |
| 1.3.3 | Nonlinear coefficient (α) | 4 |
| 1.4 | Literature review | 5 |
| 1.5 | Aim of the work | 7 |
| | CHAPTER TWO (THEORICAL) | |
| 2.1 | Crystal Structures of ZnO varistor | 8 |
| 2.2 | The structure of ZnO based varistor | 9 |
| 2.2.1 | Semiconductor ZnO grains | 10 |
| 2.2.2 | Bi-rich phase | 10 |
| 2.3 | The behavior of ZnO varistors and electrical regions | 12 |
| 2.4 | The electrical conduction in metals and semiconductors | 15 |
| 2.5 | Some electrical properties of ZnO varistor | 15 |
| 2.5.1 | Non Linear coefficient (α) | 15 |
| 2.5.2 | The Leakage current (I_L) | 15 |
| 2.5.3 | The breakdown voltage (v_b) | 16 |
| 2.5.4 | The dielectric properties | 16 |
| 2.5.5 | The average grain size | 17 |
| 2.6 | The effect of additive on the characteristics of ZnO varistor | 17 |
| 2.7 | sintering process | 18 |
| 2.7.1 | Variables sintering effects | 18 |
| 2.7.2 | Sintering type | 19 |
| 2.7.3 | Sintering influence on ZnO varistor's characteristics | 20 |
| 2.8 | X-ray diffraction testing | 20 |
| 2.9 | SEM test | 22 |
| | | |

| No. | Subject | Page |
|--|---|------|
| CHAPTER THREE SAMPLES PREPARATION | | |
| 3.1 | Introduction of the work | 23 |
| 3.2 | Samples prepare | 23 |
| 3.2.1 | Preparing of the material | 24 |
| 3.2.2 | Weighting | 25 |
| 3.2.3 | Mixing | 27 |
| 3.2.4 | Drying | 27 |
| 3.2.5 | Calcination | 27 |
| 3.2.6 | Milling | 28 |
| 3.2.7 | The samples forming | 28 |
| 3.2.8 | Sintering process | 29 |
| 3.2.9 | Polishing process | 30 |
| 3.2.10 | Electrodes | 31 |
| 3.3 | X-Ray diffraction test | 31 |
| 3.4 | Measurement of electrical characteristics | 32 |
| 3.4.1 | Breakdown voltage (V_b) | 32 |
| 3.4.2 | Leakage current (I_L) | 33 |
| 3.4.3 | Nonlinear coefficient (α) | 33 |
| 3.4.4 | Dielectric features test | 33 |
| 3.5 | SEM test | 34 |
| 3.6 | Optical I-V property measurement | 35 |
| CHAPTER FOUR RESULTS AND DISCUSSION | | |
| 4.1 | Introduction | 36 |
| 4.2 | XRD results | 36 |
| 4.3 | The calculation of crystallite size | 41 |
| 4.4 | SEM test | 42 |
| 4.5 | The electrical mensuration | 45 |
| 4.5.1 | Breakdown voltage (V_b) | 45 |
| 4.5.2 | leakage current (I_L) | 49 |
| 4.5.3 | The nonlinear coefficient (α) | 52 |
| 4.5.4 | Dielectric constant (ϵ) | 58 |
| 4.5.5 | Dissipation factor (loss factor) | 60 |
| 4.6 | I-V measurements | 62 |
| | | |

| | | |
|-----|---|----|
| | CHAPTER FIVE CONCLUSIONS AND SUGGESTIONS FOR FUTURE WORK | |
| 5.1 | Conclusion | 64 |
| 5.2 | Future Work | 64 |
| | REFERENCES | 65 |
| | | |

LIST OF FIGURES

| No. | Figure | Page |
|------------|---|-------------|
| 1.1 | Different types of ZnO varistors for distinct applications | 2 |
| 2.1 | the three of ZnO structure | 8 |
| 2.2 | the wurtzite structure of ZnO | 9 |
| 2.3 | (a) existing and (b) perfect structure of a varistor | 9 |
| 2.4 | grain and three types of grain boundaries | 11 |
| 2.5 | Zinc oxide-Bi ₂ O ₃ based polycrystalline sintering varistor and current trajectory | 12 |
| 2.6 | Current voltage graph of typical metal oxide varistors | 13 |
| 2.7 | sintering of solid state reaction | 19 |
| 2.8 | XRD principles from a number of planes | 21 |
| 2.9 | the SEM device | 22 |
| 3.1 | sketch shows the experiment work | 23 |
| 3.2 | calcination the powder | 27 |
| 3.3 | images of molds and presses | 28 |
| 3.4 | image of the furnace sintering | 29 |
| 3.5 | image of produced samples | 30 |
| 3.6 | samples images after aluminum electrode | 31 |
| 3.7 | power supply and multimeters images | 32 |
| 3.8 | LCR meter image | 33 |
| 3.9 | SEM device image | 34 |
| 4.1 | X-ray diffraction sketch for pure ZnO powder | 36 |
| 4.2 | X-ray diffraction sketch for In ₂ O ₃ nano powder | 37 |
| 4.3 | X-ray diffraction sketch for BC0 sample at 1000°C | 37 |
| 4.4 | X-ray diffraction sketch for BC1 sample at 1000°C | 38 |
| 4.5 | X-ray diffraction sketch for BC2 sample at 1000°C | 39 |
| 4.6 | X-ray diffraction sketch for BC3 sample at 1000°C | 39 |
| 4.7 | X-ray diffraction sketch for BC3 sample at 1050°C | 40 |
| 4.8 | X-ray diffraction sketch for BC3 sample at 1100°C | 40 |
| 4.9.a | SEM image for (BC0) sample sintered at (1000) °C | 42 |
| 4.9.b | SEM image for (BC3) sample sintered at (1000) °C | 43 |
| 4.9.c | SEM image for (BC3) sample sintered at (1050) °C | 43 |
| 4.9.d | SEM image for (BC3) sample sintered at (1100) °C | 44 |
| 4.10 | divergence of breakdown voltage with increased In ₂ O ₃ % mol concentration at 1000°C | 47 |
| 4.11 | divergence of breakdown voltage with increased In ₂ O ₃ % mol concentration at 1000°C | 47 |

| No. | Figure | Page |
|------|---|------|
| 4.12 | divergence of breakdown voltage with increased In ₂ O ₃ % mol concentration at 1100°C | 48 |
| 4.13 | divergence of the leakage current with increased In ₂ O ₃ % mol concentration at 1000°C | 50 |
| 4.14 | divergence of the leakage current with increased In ₂ O ₃ % mol concentration at 1050°C | 50 |
| 4.15 | divergence of the leakage current with increased In ₂ O ₃ % mol concentration at 1100°C | 51 |
| 4.16 | I-V curve for 1000°C samples | 53 |
| 4.17 | I-V curve for 1050°C samples | 54 |
| 4.18 | I-V curve for 1100°C samples | 55 |
| 4.19 | divergence of the nonlinear coefficient with increased In ₂ O ₃ % mol concentration at 1000°C | 56 |
| 4.20 | divergence of the nonlinear coefficient with increased In ₂ O ₃ % mol concentration at 1050°C | 57 |
| 4.21 | divergence of the nonlinear coefficient with increased In ₂ O ₃ % mol concentration at 1100°C | 57 |
| 4.22 | Dielectric constant for (BC0, BC1, BC2 and BC3) as a frequency function sintered at 1050°C | 58 |
| 4.23 | Dielectric constant for (BC1 and BC3) as a frequency function sintered at 1100°C | 59 |
| 4.24 | loss factor for (BC0, BC1, BC2 and BC3) as a frequency function sintered at 1050°C | 60 |
| 4.25 | loss factor for (BC1 and BC3) as a frequency function sintered at 1100°C | 61 |
| 4.26 | I-V test curve for 1000°C sample (BC0) at light and darkness | 62 |
| 4.27 | I-V test curve for 1000°C sample (BC3) at light and darkness | 62 |
| 4.28 | I-V test curve for 1050°C sample (BC3) at light and darkness | 63 |
| 4.29 | I-V test curve for 1100°C sample (BC3) at light and darkness | 63 |
| | | |
| | | |
| | | |
| | | |
| | | |
| | | |
| | | |

LIST OF TABLES

| No. | Table | Page |
|------------|---|-------------|
| 3.1 | The major features of starting materials | 24 |
| 3.2 | molar mass, molar ratio and 30% mass of the composition | 25 |
| 4.1 | crystallite size of different samples with different sintering temperatures | 41 |
| 4.2 | shows the diameter of some grains of the samples, wich determined by SEM | 44 |
| 4.3 | the measured of (V_b) of the samples | 46 |
| 4.4 | leakage current measurments for all samples | 49 |
| 4.5 | nonlinear coefficient values for all samples | 52 |

| SYMBOLS | MEANING |
|--------------|--|
| α | Non-linear coefficient |
| K | Constant |
| I | Current |
| V | Voltage |
| c | Constant |
| R | Ohmic resistance |
| R_D | Differential resistance |
| V_b | Breakdown voltage |
| I_L | Leakage current |
| D | Average grain size |
| JCPDS | Joint Committee on Powder Diffraction Standard |
| hcp | hexagonal–close–pack |
| λ | Wave length |
| θ | Bragg angle |
| β | Full width at half maximum |
| SEM | Scanning Electron Microscopy |
| ϵ' | Real dielectric constant |
| ϵ'' | Imaging dielectric constant |
| ϵ_0 | The permittivity of vacuum. |
| d | The varistor sample thickness |
| | |

CHAPTER ONE

INTRODUCTION

(1-1) Introduction

Zinc oxide is an organic compound with the chemical formula ZnO. It is a white powder, poor solubility in water. In particular this oxide is widely used as an additive to many industrial materials including ceramics, plastics, glass and cement [1].

Zinc oxides (ZnO), has recently been given widespread attention due to their low resistance, excellent conductivity, high transparency and nontoxic properties [2].

It is characterized by its low cost compared to the rest of the oxides with a wide energy gap about 3.37eV at a temperature of (300k) and 3.44eV at low temperatures and it is classified as n-type semiconductor. Thus it has been used in varistor electrical and optical applications such as piezoelectric transducer, and gas sensor [3].

The metal oxide ZnO - based varistor (MOV), is a semiconductor device made of ceramic which has perfect non-linear characteristic whose applications are technologically important when they are normally connected in parallel with an electric devices, and that is most used to protect the electric devices and electronic circuits from dangerous of over-voltages that may cause by a lightning strike or electrostatic discharge [4].

At low voltage, varistors work as resistors, and they become conductors at high voltage. Unlike the fuse or circuit breaker, that act as protector against over-current, the varistor functions as an over-voltage depending resistor. Moreover the resistance is adjustable with the applied voltage [5].

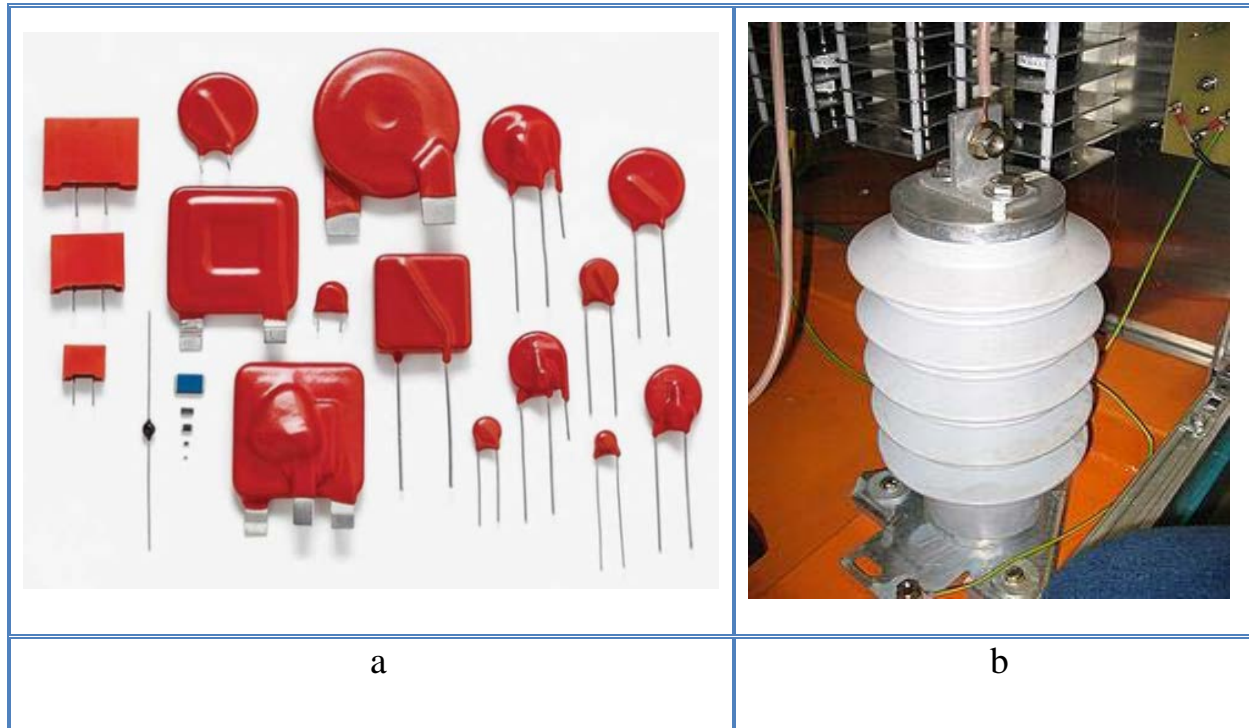


Figure (1-1) Different types of ZnO varistors for distinct applications [5]:

a-Low-voltage suppression varistors, b- High voltage protection varistors

Over the past 60 years, the varistors become the best protection ways of electronic and power distribution and transmission circuits [6]

(1-2) ZnO varistor composition

In the beginning metal oxide varistors have been highly complex and characterized as polycrystalline ceramics. They consist of 90% zinc oxide as a ceramic-based material which are adding and mixing with small amount of other oxides for example, Bi_2O_3 , CoO , Sb_2O_3 , Cr_2O_3 , MnO_2 and SiO_2 in certain molar to improve and enhance the non-ohmic characteristic of the varistor [7].

These oxides influence the varistor characteristics by separate at grain boundaries of ZnO and make a stratum of intergranular phase like bismuth or by an effect on development of growth the grains and structure of varistor. After sintering process, the varistor will be shaped as a mold with elevated resistivity conductive ZnO grain boundaries (intergranular insulating layers) create schottky barriers at electrically active grain boundaries [8].

These barriers appear at the limit of each (n-type) semiconducting ZnO grain from the electrons boundary and they respond to the varistor's electrical and non-ohmic characteristics. Therefore the varistor has ability to provide a described sequence and parallel connection of grain boundaries, each having 3V breakdown voltage. This creates a structure made up of conductive enormous granules of ZnO surrounded by thin electrically insulating barriers [9].

The microstructure of doped zinc oxide varistors is a polycrystalline composed of numerous semiconducting zinc oxide grains and grain boundaries [10].

(1-3) Some of the varistor electric properties

(1-3-1) The leakage current (I_L)

The current passes through the varistor, while the circuit is functioning normal work as a protection [11].

The current measurement is possible at point when the voltages are equal to $(0.8) V_b$ [9].

(1-3-2) Break down voltage (Varistor voltage)

When 0.5mA of current is applied, the voltage passes through the varistor. At this voltages value, the varistor will begin to transform from insulating to conducting condition [9].

(1-3-3) Non-linear coefficient (α)

It refer to the degrees of varistor's non-linearity and it defines the varistor sensory potential and immediately limits the high voltage surge. The electrical properties of varistor significantly depend on the composition and the structure i.e. grains, second phase distribution, and density [12].

Consequently, in order to improve the electrical properties of ZnO varistor it is necessary to get {less leakage current, higher non-linear coefficient (low responding time) and appropriate breakdown voltage (V_b) of certain enforcement. Controlling sintering condition and homogenization are quite important as they lead to a better allocation [13].

In addition the development of grain size can be regulated by the sintering environment. However, (v_b) depends on the amount of grain boundaries adjusted by the size and grain thickness [14].

The electrical conductivity is due to the addition of many different compounds , with the expect for ZnO which tends to form n-type semiconductor material in which the electrical conductivity is due to ZnO with expect interstitially inside the lattice and in oxygen vacancies [15].

(1-4) Literature review

- In (2006) M. Žunić, Z. Branković and G. Branković prepared the Zinc oxide varistor by immediate mixing of constituent phases with study the impact of minor phases like (spinel and intergranular) on electrical characteristic. Then prove that property changes rely on the relative molar ratio of the phases [16].

- In (2010) Xu dong , et. al. doped (Lu_2O_3) with ($\text{ZnO-Bi}_2\text{O}_3$) based varistor that prepared by using solid state reaction and heat sintering at (900, 950 and 1000) °C. The outcomes showed the additive of (0.3% Lu_2O_3) which sintered at (950 °C) display the perfect electrical characteristic of varistor [17].

- In (2011) Mariem Chaari et al. studied the influence of increase of sintering temperature on ZnO based varistor. The results found (by using of AFM and SEM tests) that increases the grain size and surface roughness at the increase of sintering temperature, and the samples obtained have polycrystalline hexagonal structure [18].

- In (2012) A. Yaya , et. al. Investigated the consequence doping the (Sb_2O_3 and Bi_2O_3) on structure and electrical characteristic of Zinc Oxide varistor.

The result present that Bi_2O_3 doping inhibited the grain growth of Zinc oxide and enhanced the electrical characteristic of varistor [8].

- In (2012) Chenghua Zhang, et. Al. researched the structure and electrical conduct of ($\text{Bi}_2\text{O}_3\text{-ZnO}$) - based varistor that prepared for distinct five times (0, 1, 3, 5 and 10) hours by high-energy ball milling [19].

The XRD patterns of the samples (that shown in appendix)

- In (2013) Ji-Leli, et. al. they doped Y_2O_3 and Nd_2O_3 with ZnO based varistor and discussed the phase composition, structure, and electrical characteristic of the varistor. The results displayed that (0.1 mol % of Y_2O_3) and (0.25 mol% of Nd_2O_3) doped to the ZnO varistor with sintering heat ($1050\text{ }^\circ\text{C}$) improved the electrical characteristic with higher breakdown field (556.4V/mm), the non-linear coefficient amount of (61) and the leakage current density about ($1.55\text{ }\mu\text{A/Cm}^2$) [20].

- In (2013) Lei Ke, et. al. investigated the rare earth material influence and non- high temperature of sintering on electrical conduct of Zinc oxide varistor the result displayed that after doping (0.08 mol% Y_2O_3) at ($800^\circ\text{C} - 2\text{h}$) sintring. the breakdown field increases to (2247.2V/mm) [21].

- In (2014) Abdel- Mageed H. Khafagy, et. al. discussed the impact on electrical characteristics, structure and hardness of Mn_3O_4 doping of ZVM (Vanadium oxide doped Zinc oxide varistor). The result displayed that added (0.5 mol % Mn_3O_4), will reduced grain size to $19.55\text{ }\mu\text{m}$ and nonlinearity of varistor about (16.29) with leakage current density about ($441.9\text{ }\mu\text{A/Cm}^2$) [22].

- In (2015) Adil Ismaeel Khadim studied the ZnO varistor behavior by doping with many metal oxides and tested their effect alone then added the rare earth oxides (M_2O_3). The outcomes explained at increase the sintering temperature the unit cell size will increase, the nonlinear coefficient decrease above (1100°C) sintering temperature, and the leakage current increased with increasing the sintering temperature [3].

- In (2016) Abbas Fadhel Shannoon prepared the ZnO varistor by mixing some metal oxides and doping with (Al_2O_3) and study the electrical properties. The results showed that crystallite size was increased with the increase of sintering temperature, and (the breakdown voltage, the nonlinear coefficient and Deilectric constant) decreased with the increase of sintering temperature [23].

- In (2018) Zainab Waleed Ahmed. Studied the Electrical Properties of varistor ceramic composite by mixing based (ZnO) with some oxides with sintering temperatures (1050°C, 1100°C and 1150°C) [24].

(1-5) Aim of the work

The aim of this work is to enhanced the varistor properties by prepare ZnO-based varistor sampels by solid state reaction with some metal oxides with molar ratios of (In₂O₃) nano powder additive with different sintering temperatures. And study the effect of these molar ratios of (In₂O₃) nano powder additive on electrical properties of varistor.

CHAPTER TWO

THEORY

(2-1) Crystal Structures of ZnO varistor

Because of the Zinc oxide has a wide band gap around (3.37) ev, it is (II-VI) a combination n-type semiconductor, known as technology material and used in applications in industry and technology [25, 26]. ZnO has three structures according to the conditions of crystallization they are: wurtzite, Zinc blend and rocksalt, that shown in figure (2-1)

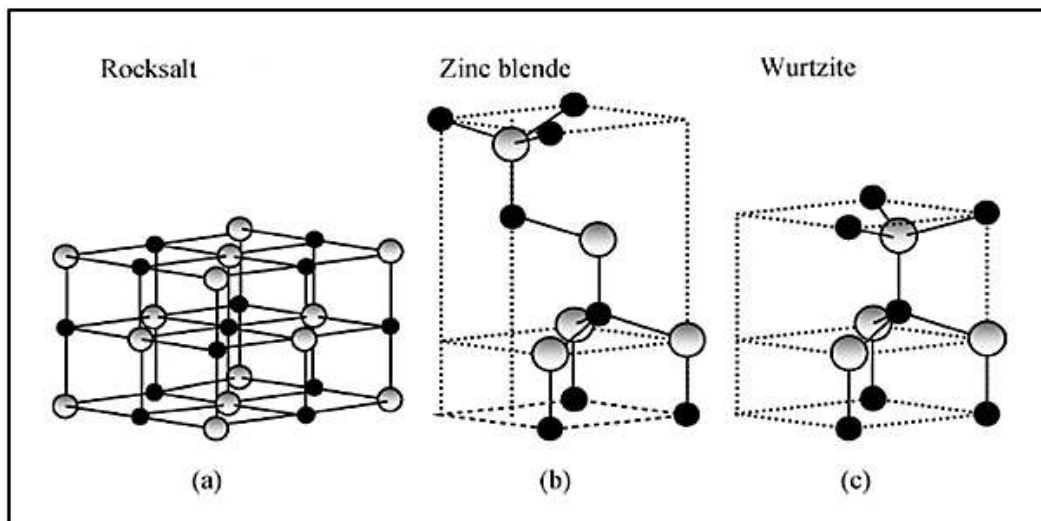


Figure (2-1) the three of ZnO structure, which are [27]:

a) Cubic rocksalt, b) Cubic zinc blende and c) Hexagonal wurtzite

The rocksalt structure maybe found at high pressures about (10 Gpa) [28]. By growing ZnO on a cubic lattice structure substratum, zinc blende can be acquired. The wurtzite is the common ZnO structure because its stability at ambient condition, with hexagonal cell with parameter for the lattice

($a = 3.25 \text{ \AA}$) and ($C = 5.12 \text{ \AA}$)

This structure has two inter-penetrating and alternately c-axis hexagonal – close – pack (hcp) sub lattices, which mean a number of (Zn) atoms and (O) atomic planes, which are stacked instead of along a C axis [29,30].

Every Zinc cation (Zn^{+2} with radius about 0.074 nm) is enclitic by four oxygen anions (O^{-2}) to form a tetrahedral structure, with covalent bands in the c-direction between the zinc and oxygen atoms, while it is ionic in a-direction, so ZnO crystals behaves differently in properties, as shown in figure (2-2) [31].

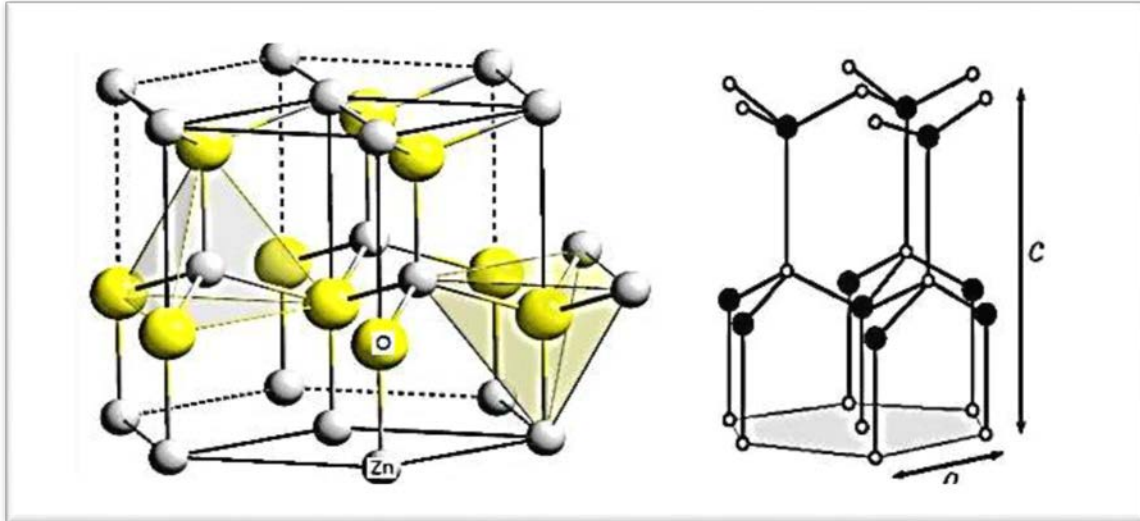


Figure (2-2) the wurtzite structure of ZnO

(2-2)The structure of ZnO based varistor

The electrical characteristics (non-linear characteristics) of the Zinc oxide varistor depends on chemical and structure parameters (grain size, morphology and density).The conventional Zinc oxide- based varistor is based with some molar metal oxides like (Sb_2O_3 , Bi_2O_3 , CoO , Mn_2O_3 , and etc) [32].

The zinc oxide powder produces a poly-crystallizing ceramic during the liquid phase sintering process, composed of n-type ZnO semi-conductor with a small strength detached from a resistive grain boundaries which is characteristic of a double Schottky-barrier [33], and this shown in figure (2-3).

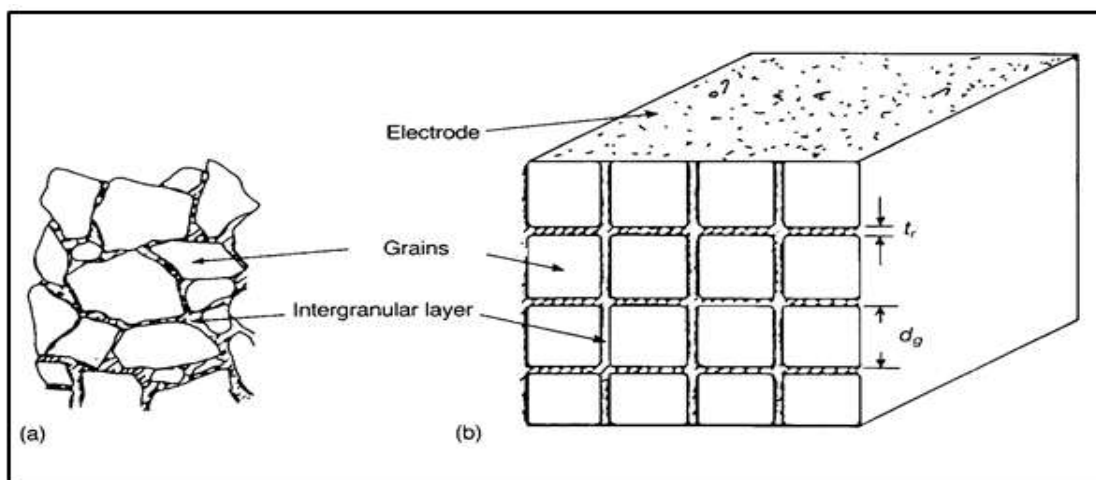


Figure (2-3): (a) existing and (b) perfect structure of a varistor [34]

Anyway, the exemplary microstructure of ceramic varistors contains:-

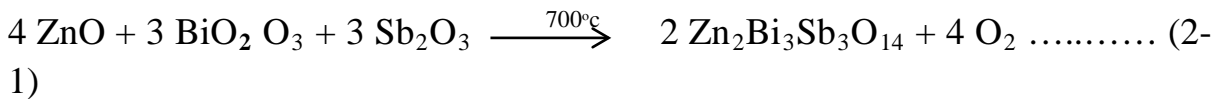
(2-2-1) Semiconductor ZnO grains:-

Represent the basic building block of varistor, and they are very similar in chemical composition, but differ a lot in geometry. The ZnO grain size depends on the material composition and sintering [32, 35].

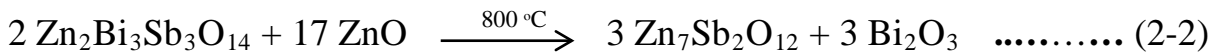
(2-2-2) Bi-rich phase:-

This stage creates an open 3-dimensional lattice form in which the Zinc oxide grains inserted. This stage contains many kinds of crystalline phases like (different polymorphs of Bi₂O₃, a Pyrochlore phase (Zn₂Bi₃Sb₃O₁₄), and spinel phase (Zn₇Sb₂O₁₂)).

Pyrochlore –phase creates when Bi₂O₃ reacts at sintering temperatures above 700°C with ZnO and Sb₂O₃ owing the equation:



When the sintering temperature rises more than (800°C) Pyrochlore takes a spinel phase because of this equation:-



In ZnO microstructure, other spinel crystal stages can be created like (ZnIn₂O₄) when varistor based on ZnO doped with (In₂O₃), these phases formed the ZnO varistor grain boundaries [32,8].

So we can classify the grain boundaries into three types [36]:

Type 1: It has a thick layer of amorphous Bi₂O₃-rich and can contain tiny secondary-phase crystallites like spinel and pyrochlore. The thickness of this layer is above (100 nm) and has no function in electrical conductivity, but by Pinning the grain boundaries inhibits grain growth to create a consistent distribution of ZnO grain size.

Type 2: Limits of thin grain boundaries (1-100 nm) with an amorphous intergranular layer of only Bi₂O₃-rich.

Type 3: Direct ZnO grain contact without intergranular contact between ZnO grains but some ions such as (Bi, Co, O) can be identified at about several nanometers in thickness.

All these types are shown in figure (2-4)

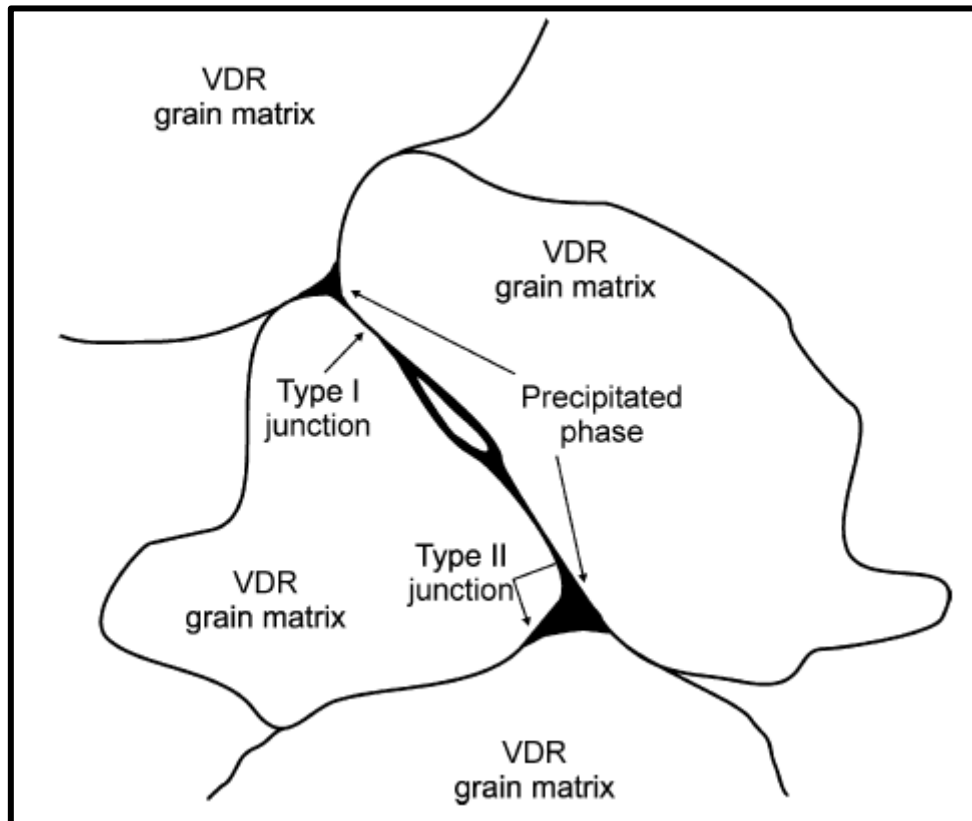


Figure (2-4): grain and three types of grain boundaries [36]

Lack of spinel phase raises the boundaries of active grain, so kinds (2 and 3) are the sources of nonlinear varistor characteristics, and represent the active grain boundaries that the electric current flows through [9], as shown in figure (2-5)

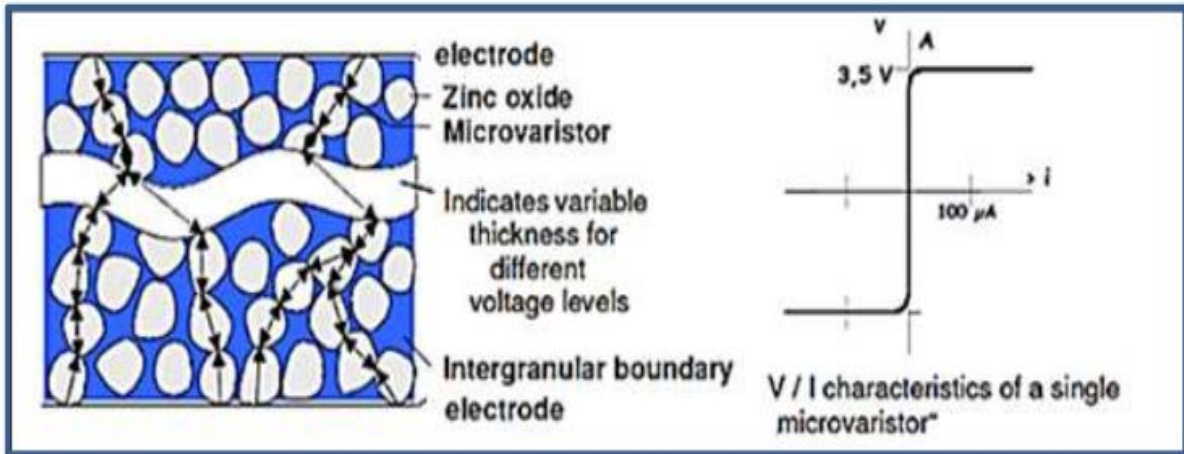


Figure (2-5): Zinc oxide-Bi₂O₃ based polycrystalline sintering varistor and current trajectory [37]

(2-3)The behavior of Zinc oxide varistors and electrical regions:

ZnO varistors are multi-phase, polycrystalline, doped, metal oxide and solid-state ceramics. ZnO and other metal oxide additives such as antimony, bismuth, cobalt, manganese and nickel etc, are produced varistors. And the non-linear (non-ohmic) function of their electrical resistance to the applied voltage.

Their unique non-linear electrical characteristics come from the internal interfaces between ZnO grains and the ceramic grain boundaries. The ZnO varistor has a very steep nonlinear current-voltage curve and can therefore support very varied currents across a narrow voltage range, this phenomenon is called (The varistor effect).

The varistor behaves as an open circuit at low voltages beyond the voltage breakdown, V_b becomes a short circuit protecting the parallel connected component or components. The total relationship between current and voltage within a varistor leads to three different operating regions, each with a special conduction method [38, 39, 40]. The current voltage properties of a typical varistor is shown in Figure (2-6).

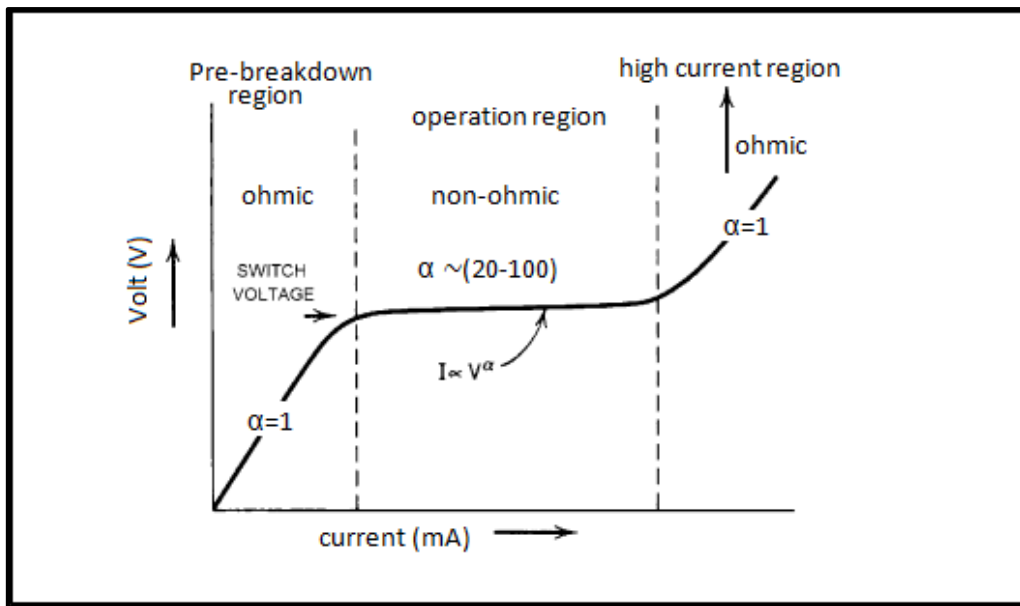


Figure (2-6) Current voltage graph of typical metal oxide varistors [41]

These three regions can be classified to:

Zone 1: Leakage region (pre-breakdown region): varistor is highly resistant in the range of $10^{12} \Omega cm$ at low voltages and can be seen as an excellent insulating device [42,43] .

In this region, Ohm's law describes the current voltage behavior of the varistor and controls its grain boundary resistivity, which is consistent with the varistor, operation without any high voltage, (the region of pre-breakdown determines the steady state joule heating and the varistor nominal voltage), the leakage current is a temperature function, that is, increases as the temperature increases [44,45].

Zone 2: Breakdown region (action region): If the voltage exceeds a certain value, often known as the breakdown voltage or breakdown field, the varistor is highly conductive and leads an increasing amount of current for a small voltage increase, the device's resistivity in this region drops dramatically to 1-10 Ωcm . And Ohm's Law can no longer describe the current voltage properties.

The relationship between current and voltage is generally expressed by the empirical power equation of varistors: [46,47].

$$I = \left(\frac{V}{C}\right)^\alpha \dots\dots\dots (2-3)$$

$$K = \left(\frac{1}{C}\right)^\alpha \dots\dots\dots (2-4)$$

If ($\alpha = 1$) is simplified with the law of Ohm, then the current is proportional to the voltage applied. The device acts like an Ohms resistor in this case [46].

When ($\alpha = \infty$) for minor changes in the applied field in the proximity of the breakdown voltage, the current varied infinitely, and the device will be perfect. The varistors in practice work between a perfect varistor and an ohmic resistor. The higher of the (ϕ), the better the device and the greater the degree of protection [43,48].

$$\text{And } \alpha = \frac{R}{R_D} \dots\dots\dots (2-5)$$

Where R = ohmic resistance and R_D = differential resistance.

$$\alpha = \frac{R}{R_D} = \frac{V/I}{dV/dI} \dots\dots\dots (2-6)$$

$$\alpha = \frac{V/I}{dV/dI} = \frac{dI/I}{dV/V} \dots\dots\dots (2-7)$$

$$\alpha = \frac{\int dI/I}{\int dV/V} \dots\dots\dots (2-8)$$

$$\alpha = \frac{\log I_2 - \log I_1}{\log V_2 - \log V_1} \dots\dots\dots (2-9)$$

Where, ϕ = the degree of nonlinearity or nonlinear coefficient, V = the applied voltage, I = the current passing through the device, C is a constant. And on the application of transient surge the nonlinear region determines the clamping voltage, and this region is the varistor heart. In this area the current voltage properties are practically temperature independent [49,21].

Zone 3: (Upturn region): Again the current voltage of varistors shows another very high current Ohmic region, that is happens at current densities of about (10^3 A/cm^2). This area is often called an upturn area where the current increases again linearly with the voltage [47,50].

(2-4)The electrical conduction in metals and semiconductors:

Metals and semiconductor's electrical conduction varies considerably, and the resistance of the two materials depends on the temperature. The resistance in semiconductors reduce as their temperature rises, but the reverse is in the metals. The electrons move up to a greater energy level and experience big numbers of collisions per unit time when temperature increase and reduce time between collisions, thereby increasing metal resistance [51].

In a semiconductor, two charging carriers are available: the valence band holes and the conduction band electrons, if the temperature rises, the valence electron can acquire energy to reach the conductive band, that made holes (empty states), This mean increases the amount of carriers and reduces the resistance of semiconductors [52].

(2-5) Some electrical properties of ZnO varistor

(2-5-1) Non Linear coefficient (α):

The most significant parameter of the ZnO varistor is the nonlinear coefficient (α) and the degree of the nonlinearity of electric conductivity and determines Zinc oxide varistor ability to repress voltage surges instantaneously [53]. Since ZnO varistor's nonlinear behavior owing to the phenomenon of grain boundaries [54]. In particular additives, homogenization and sintering conditions must be controlled by processing parameters to obtain a regular microstructure [16].

(2-5-2) The Leakage current (I_L):

One of the significant parameters for ZnO varistor is the leakage current due to It determines the quantity of loss the power of electricity at the Pre-breakdown area (ordinary voltage) which looks like a heat, so reduced of the leakage current lead the varistor to be better [55].

The elevated leakage current rate can heat the devices and influence other electrical characteristics. If the heat is not transferred to the outside atmosphere due to the leakage current, It can cause the device to run thermally away. So, the manufacturer's direction is to reduce the leakage current to the lowest possible level [56].

The leakage current can be measure as: [46].

$$I_L = I_{0.1mA} \dots\dots\dots (2-10)$$

(2-5-3)The breakdown voltage (v_b)

The voltage at which the nonlinearity starts and it refers to that the device changes from insulating to conducting rule. It is described as the voltage that the device passes under (0.5 mA) of current and is referred to as V_{0.5}. The steady-state voltage of the circuit is set to a certain proportion of breakdown voltage, ordinarily in power implementation and it is set at (70 to 80) % of (V_{0.5 mA}), as shown by the following equation: [47].

$$V_b = 0.8 V_{0.5 mA} \dots\dots\dots (2-11)$$

(2-5-4)The dielectric properties:

Since the varistor functions in the breakdown (low current region) conduct like an insulator (dielectric material), it has dielectric characteristics that also include true dielectric constant, imaginary dielectric constant (loss factor).

We can calculate true dielectric constant (ε') from equation:

$$\epsilon' = C \cdot d / \epsilon_0 A \dots\dots\dots (2-12)$$

Where:

C: The varistor's capacity , ε₀: The Vacuum permittivity

d: The varistor sample thickness , A: The sample cross-sectional region

We can calculate the imaginary dielectric constant ε'' (dielectric loos) by the equation:

$$\epsilon'' = \epsilon' \tan\delta \dots\dots\dots (2-13)$$

Where: tanδ refers to the proportion of real and imaginary dielectric constant [57].

(2-5-5)The average grain size:

To determined the average grain size we can use the Scherer equation from X-Ray diffraction information as follows [58]:

$$D = \frac{K \lambda}{\beta(2\theta)\cos\theta} \dots\dots\dots (2-14)$$

Where: D: refer to grain size (nm)

λ : is the incident X-ray beam wavelength= (1.54 Å)

k: is constant= 0.94

β ; is full width at half maximum (radians) FWHM

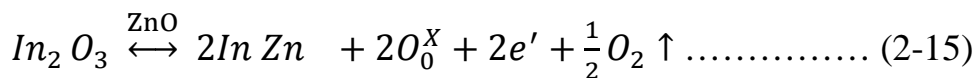
θ : is Bragg angle (peak position)

(2-6) The effect of additive on the characteristics of ZnO varistor:

Several kinds of additives such as (Bi₂O₃, Sb₂O₃, Cr₂O₃, CoO, MnO₂ and In₂O₃) and other metal oxides are added to acquire the non-ohmic feature of the ZnO varistor into a certain molar proportion [59]. Each of these dopants has a special role to enhancing ZnO varistor's electrical properties [60].

(Bi₂O₃) is the basic dopant caused by ZnO varistor's nonlinear characteristic, it has a melting point of (825°C) composes a liquid phase during the sintering process that enables other dopants to be transferred between grains And then segregates at the znO grain boundaries producing a highly charged layer causing an electrostatic barrier that induces nonlinearity of the ZnO varistor [61,8].

Also the (In₂O₃) is a spinal phase (ZnIn₂O₄) that performs the same function as other spinal phase by inhibit the grain growth [36]. Due to the fact that Indium is a donor dopant, the electrical conductivity of ZnO grains is increased by dissolving certain Indium atoms in the ZnO crystal lattice.



In this state, the ZnO grains are transported from the semiconductor to the metallic conduct.

Cr₂O₃, CoO and MnO₂ improve ZnO varistor's nonlinear characteristics, because transition metal oxides are thought to be important to create an electrostatic barrier at the boundaries of the ZnO varistor grain [62].

(2-7) sintering process

Ceramic most products are made of powder technology and bulk ceramic parts are always mechanically poor. Ceramic materials are generally manufactured use a heat treatment step to form the needed shape, this is called sintering process from powder and transformed to a thick solid, Which can be the most significant step in a solid state reaction [63,64].

This process can be defined as a processing technique for material and part manufacturing with high ceramic powder or metal density Using regulated amounts and ranges of thermal energy [63]. Generally, the aims of sintering are [65]:

1. Produce a portion with design microstructure (control the grain, pores and other phases of form, size and size distribution) by regulating the variables of sintering.
2. Obtain the physical-mechanical characteristics that required and enhance strength, hardness and toughness of fractures.
3. Changes in the materials electrical and thermal conductivity

(2-7-1) Variables sintering effects:

The sintering process is regulated by a big amount of variables that determined the structure and characteristics of the sintereing, the variables may be classified into two classifications of compact powder:-

1. Variables of materials: the raw material variable that includes:

(Chemical composition, shape, size, size distribution, impurity, homogeneity, etc), these factors affect the density of the powder and the growth of grains.

2. Variables of processes: Include temperature, atmosphere, pressure, time, heating and cooling variables [64].

(2-7-2) Sintering type

It is possible to recognize two significant kinds of sintering which relied on the fired structure and the second phases that were created during the heat treatment:

1- Solid state sintering: It happens when the green body (compact powder) is typically heated (50% - 90%) of the melting point. The particles are bonded in this mechanism forming of the necks (particle shape changes) [66].

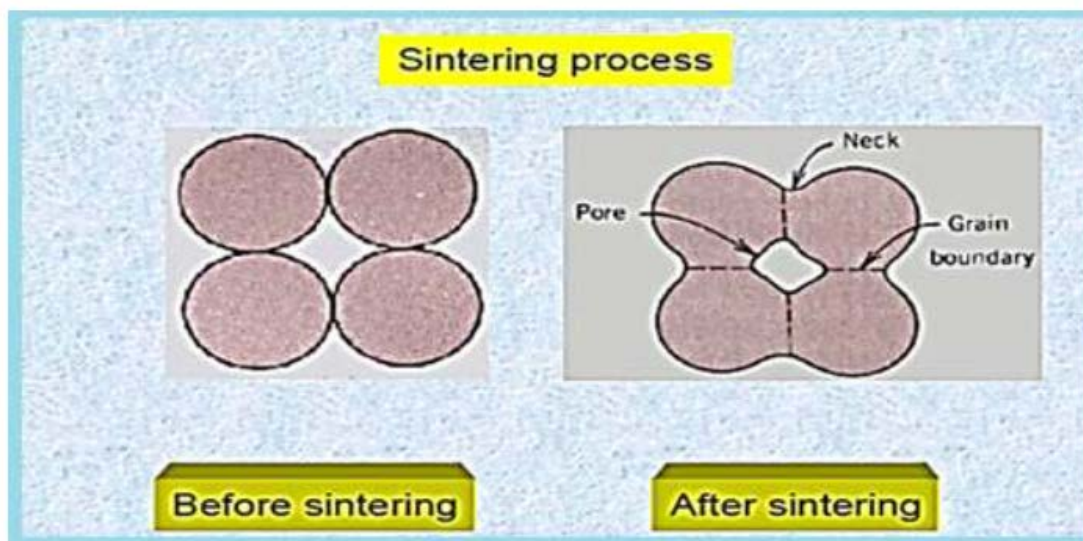


Figure (2-7) sintering of solid state reaction

2. Sintering of the liquid phase: It happens at a temperature higher than one or two of the components melting temperature of the combination of powder.

The liquid sintering phase is used to increase the rate of densification, and accelerate the growth of grains to produce different grain boundary characteristics [67].

(2-7-3) Sintering influence on ZnO varistor's microstructure and electrical characteristics:

Typically ZnO varistors are produced through standard ceramic processing (mixing, drying, forming and sintering). The chemical composition and production method particularly the sintering steps affect the microstructure of the ZnO varistor, that controls the grain growth of ZnO varistor

The higher sintering temperature accelerates the growth of grain and reduce the amount of grain boundaries which reduce the breakdown voltage for some varistor thickness. So the sintering temperature reduction is one way to achieve the varistor at high voltage [21].

(2-8) X-ray diffraction testing:

XRD is a fast analysis method mainly used to identify the phase of a crystalline material which can provide unit cell dimensional information. The structure composition and physical properties of materials can investigate by XRD test [68].

The identification of unknown materials in the sample is an easy technique with X-ray diffraction by comparing the sample diffraction pattern observed in the X-ray by standard card of diffraction of joint committee on the powder diffraction standard as a shortcut (JCPDS) cause of every crystalline have a unique XRD pattern that use as a finger print [69,70].

A monochromatic beam is directed towards a material in the X-ray diffraction test, and the material atoms function as a scattering source, then waves scatter and constructive or destructive interference exists along these various directions.

And so on let's say only the scattered waves of beam (1) and beam (2) from level (1) and level (2) with spacing interplanar (d), as illustrated with the figure (2-8)

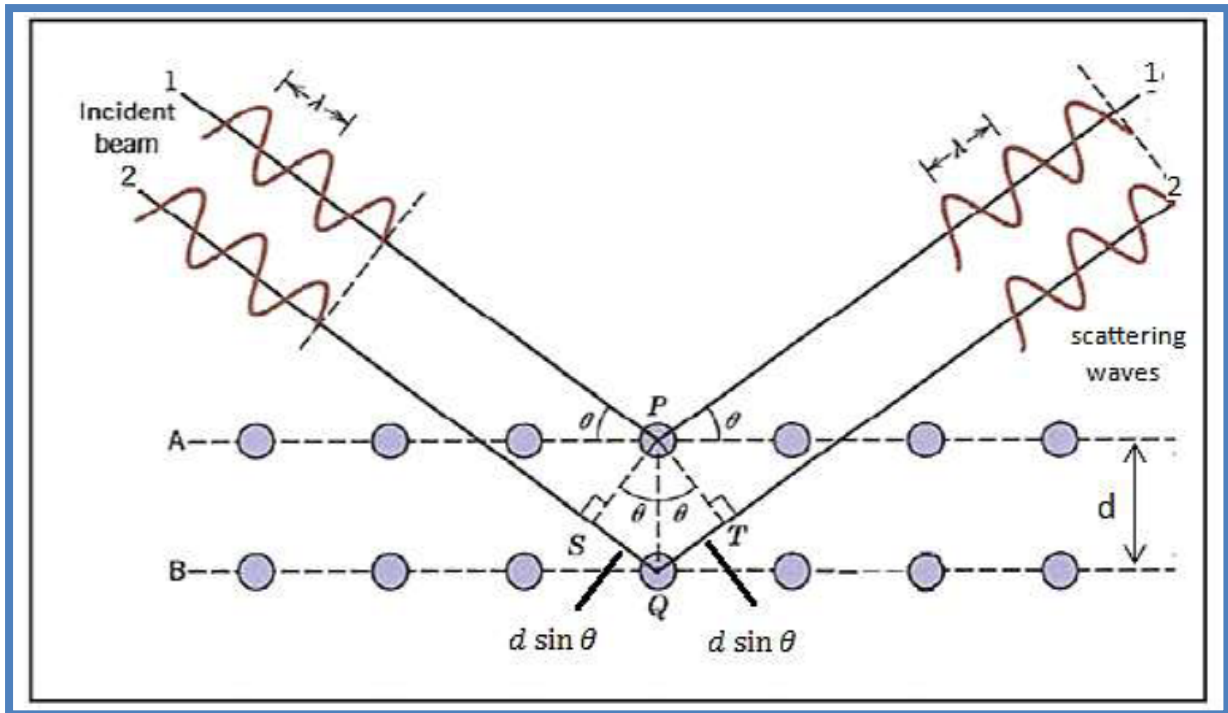


Figure (2-8) XRD principles from a number of planes [59]

The difference between (beam1) and (beam2) in the trajectory length is equal to $(2d \sin \theta)$. Constructive interference with the wave usually occurs when $(2d \sin \theta)$ multiple of one wavelength (λ) is equal to integer [71].

$$n\lambda = 2d \sin \theta \dots\dots\dots (2-16)$$

Where:

θ : The angle between the reflecting plane and the XRD beam

λ : The wavelength of XRD

(2-9) SEM test:

Scanning Electron Microscopy and as a shortcut (SEM) is a non-destructive test that used for high-resolution pictures compared to optical microscopy and provides useful particle size information and surface defects. SEM is dependent on a fine beam that touches a sample, a map of the surface topography is detected by the reflected electrons which shown in figure (2-9)

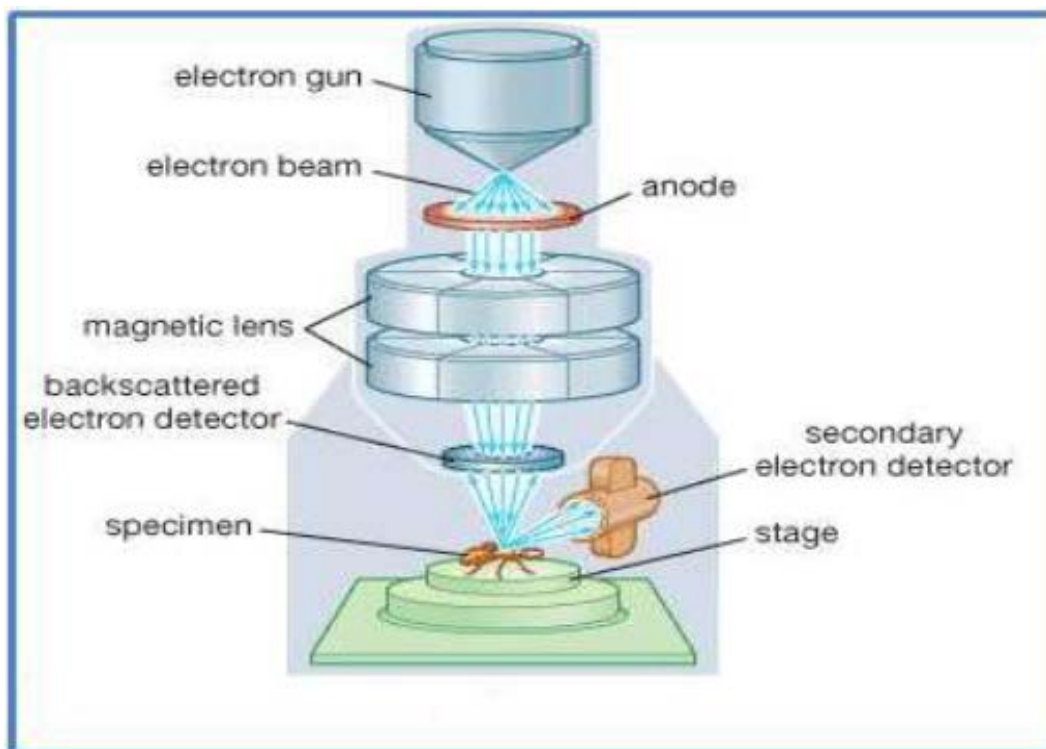


Figure (2-9) the SEM device

Particle size measurement and distribution are very important structural features to make us know how their influence on the varistor sample characteristics [72].

CHAPTER THREE

SAMPLES PREPARATION

(3-1) Introduction of the work

In the initial part of study the effect of (In₂O₃) nano powder doping on the electrical and optical properties of ZnO based varistor ,we prepared samples with four sets of various structure of (Zinc oxide-based varistor) which were sintered with various sintered temperatures they are (1000, 1050 and 1100)^o C for 2h. These samples prepared by a solid state reaction and X-ray diffraction was taken for each sample to study the results

(3-2) Samples prepare

In order to prepare a ceramic material by solid state reaction, there are several main steps that must be followed and can be represented in the following figure (3-1).

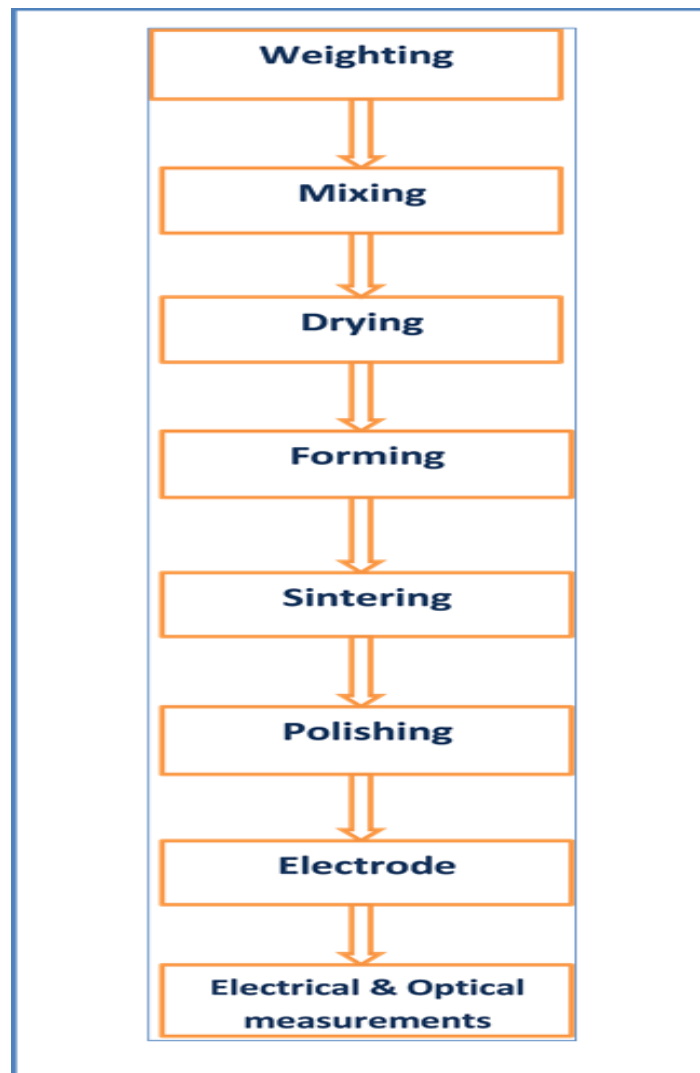









Figure (3-1) sketch shows the experiment work

(3-2-1) Preparing of the material

The beginning raw materials that used in preparing of samples shown in Table (3-1) that indicates the chemical compound, the purity, the melting point and powder images of all the starting material .

Table (3-1) the major features of starting materials

| Chemical Compound | Purity | Melting point | Image | Manufacturing |
|--------------------------------|--------|---------------|--|----------------|
| ZnO | 99% | 1975°C |  | Fluka |
| In ₂ O ₃ | 99% | 1910°C |  | GCC |
| Bi ₂ O ₃ | 99% | 817°C |  | Himeddia |
| Sb ₂ O ₃ | 99.5% | 656°C |  | Riedel-de Haën |
| MnO ₂ | 99% | 535°C |  | BDH |
| Cr ₂ O ₃ | 99.5% | 2435°C |  | BDH |
| CoO | 99.5% | 1933°C |  | BDH |

With considering test the main material (ZnO) and the doped material (In₂O₃) by X-ray diffraction test to ensure the purity ratio of the material that used in work.

(3-2-2) Weighting

To create the weights that required for making mixtures and batches for each compound, the values of the molar mass (g/mol) and mass (g) must be taken at the beginning, These values is achieved in the following relationships :

$$\text{Molar mass} = \text{element's atomic mass} \times \text{number of element's atoms} \dots\dots\dots(3-1)$$

$$\text{Mass (g)} = \text{molar mass} \left(\frac{\text{g}}{\text{mol}}\right) \times \text{molar ratio (mol)} \dots\dots\dots(3-2)$$

The values in (3-2) table which for molar mass, molar ratio and mass (g) shown with taking (30 %) of mass (g) value for each compound that prepared to a formulations (BC, BC1, BC2, BC3) where (BC) mean's batch composition.

Table (3-2) molar mass, molar ratio and 30% mass of the composition

| BC0 | | | | |
|--------------------------------|------------------------|-----------------|----------|--------------|
| chemical compound | The molar mass (g/mol) | The molar ratio | mass (g) | 30% mass (g) |
| ZnO | 81.39 | 0.965 | 78.5413 | 23.5624 |
| Bi ₂ O ₃ | 465.96 | 0.007 | 3.2617 | 0.9785 |
| Sb ₂ O ₃ | 291.52 | 0.01 | 2.9152 | 0.8745 |
| Cr ₂ O ₃ | 151.992 | 0.005 | 0.7599 | 0.2279 |
| CoO | 74.933 | 0.008 | 0.5994 | 0.1798 |
| MnO ₂ | 86.938 | 0.005 | 0.4346 | 0.1304 |
| In ₂ O ₃ | | 0 | 0 | 0 |
| | | 1 | 86.5121 | 25.9535 |

| BC1 | | | | |
|--------------------------------|------------------------|-----------------|----------|--------------|
| chemical compound | The molar mass (g/mol) | The molar ratio | mass (g) | 30% mass (g) |
| ZnO | 81.39 | 0.964 | 78.4599 | 23.5379 |
| Bi ₂ O ₃ | 465.96 | 0.007 | 3.2617 | 0.9785 |
| Sb ₂ O ₃ | 291.52 | 0.01 | 2.9152 | 0.8745 |
| Cr ₂ O ₃ | 151.992 | 0.005 | 0.7599 | 0.2279 |
| CoO | 74.933 | 0.008 | 0.5994 | 0.1798 |
| MnO ₂ | 86.938 | 0.005 | 0.4346 | 0.1304 |
| In ₂ O ₃ | 277.636 | 0.001 | 0.2776 | 0.0832 |
| | | 1 | 86.7083 | 26.0122 |

| BC2 | | | | |
|--------------------------------|------------------------|-----------------|----------|--------------|
| chemical compound | The molar mass (g/mol) | The molar ratio | mass (g) | 30% mass (g) |
| ZnO | 81.39 | 0.962 | 78.2471 | 23.4891 |
| Bi ₂ O ₃ | 465.96 | 0.007 | 3.2617 | 0.9785 |
| Sb ₂ O ₃ | 291.52 | 0.01 | 2.9152 | 0.8745 |
| Cr ₂ O ₃ | 151.992 | 0.005 | 0.7599 | 0.2279 |
| CoO | 74.933 | 0.008 | 0.5994 | 0.1798 |
| MnO ₂ | 86.938 | 0.005 | 0.4346 | 0.1304 |
| In ₂ O ₃ | 277.636 | 0.003 | 0.8329 | 0.2498 |
| | | 1 | 87.0508 | 26.13 |

| BC3 | | | | |
|--------------------------------|------------------------|-----------------|----------|--------------|
| chemical compound | The molar mass (g/mol) | The molar ratio | mass (g) | 30% mass (g) |
| ZnO | 81.39 | 0.96 | 78.1344 | 23.4403 |
| Bi ₂ O ₃ | 465.96 | 0.007 | 3.2617 | 0.9785 |
| Sb ₂ O ₃ | 291.52 | 0.01 | 2.9152 | 0.8745 |
| Cr ₂ O ₃ | 151.992 | 0.005 | 0.7599 | 0.2279 |
| CoO | 74.933 | 0.008 | 0.5994 | 0.1798 |
| MnO ₂ | 86.938 | 0.005 | 0.4346 | 0.1304 |
| In ₂ O ₃ | 277.636 | 0.005 | 1.3881 | 0.4164 |
| | | 1 | 87.4933 | 26.2478 |

(3-2-3) Mixing

The raw materials are taken after weighing to be mixed using filtered water in a bottle for a full day (24 hour) with used a magnetic electrical stirrer (England made), to get the homogeneity for samples components.

(3-2-4) Drying

After mixing process, the compound is placed in the oven at (80°C) for (24 hour) to get rid of the distilled water that used in the mixing process.

(3-2-5) Calcination:

The calcination use to get rid of gases, moisture and surface impurities of the mixed material, but before calcination process a (TGA) test was carried out to determine the phases of the oxide powders used and the temperature that would effect on them. An oven used in the atmosphere of 500°C for two hours with heating rate (5°C. min⁻¹) using ceramics crucibles in a muffle furnace, as shown in figure (3-2).



Figure (3-2) calcination the powder

(3-2-6) Milling

The combination was milled using gate mortar from the ceramic to obtain homogeneous features and particle size mixing powder.

(3-2-7) The samples forming

Compact the milled powder by pressing the disks (pellets) with pressure (250 bar), and (16 mm) diameter with thickness about (3-3.5 mm), taking into account the pressure be for equal periods of time.

Using a hydraulic Mega press (Mega company, 20 tons, Spain) with a steel mold, that shown in figure (3-3).

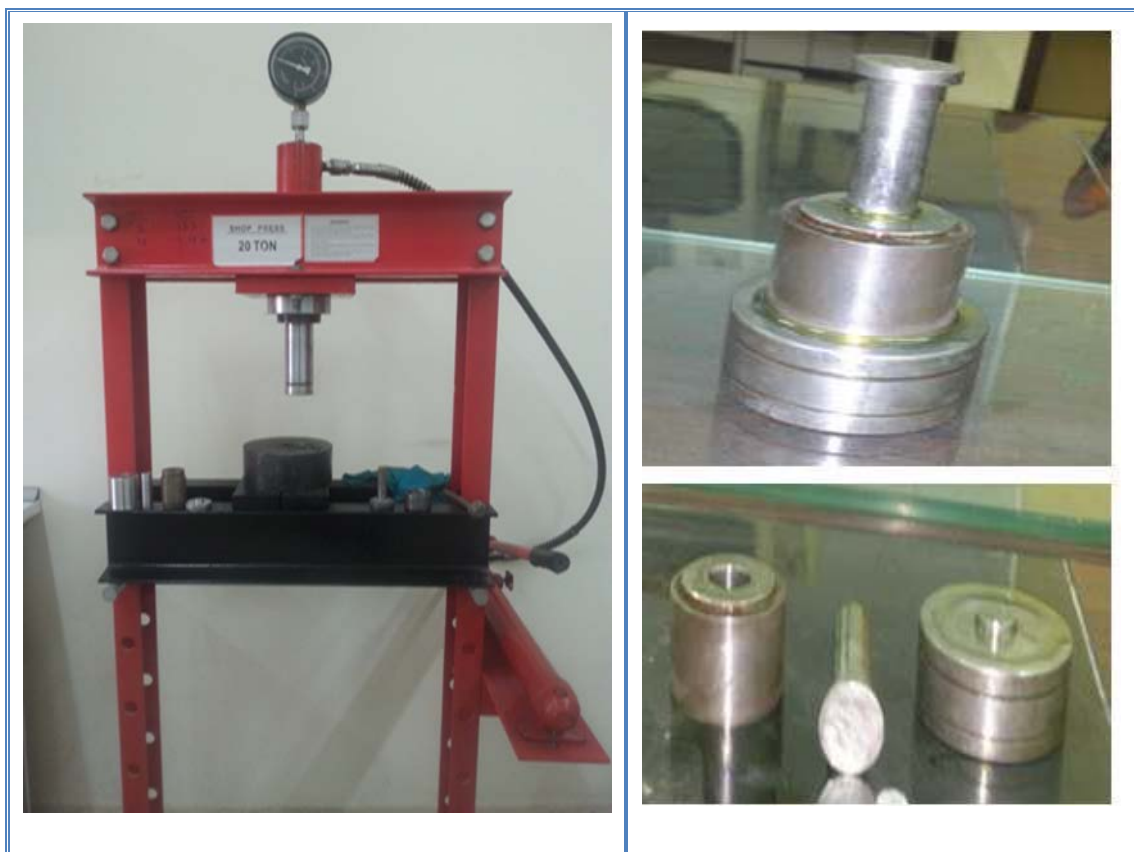


Figure (3-3) images of molds and presses

(3-2-8) Sintering process

After the pressing of green disks, use the sintering process under various temperatures to achieve of last shapes and the desired features by used the furnace, their operators explain as follow:

1. First sintering temperature (1000°C): The heating rate is equivalent to (5 °C/min) on all samples for 2 hours, and finally the furnace switched off and decreased temperature to room temperature.
2. Second sintering temperature (1050°C): The heating rate is equivalent to (5 °C/min) on all samples for 2 hours, and finally the furnace switched off and decreased temperature to room temperature.
3. Third sintering temperature (1100°C): The heating rate is equivalent to (5 °C/min) on all samples for 2 hours, and finally the furnace switched off and decreased temperature to room temperature. These processes are carried out by used the furnace that shown in the figure (3-4)



Figure (3-4) image of the furnace sintering

And the produced samples are shown in the figure (3-5)



Figure (3-5) image of produced samples

(3-2-9) Polishing process

The sample thickness and surface area effects on the structural, electrical and optical properties, so that the samples polished using different degrees of SiC abrasive papers to obtain a certain thickness.

(3-2-10) Electrodes

In this process, Electrodes were deposited to the samples using a thin film device, using aluminum element with (350 nm) of thickness with (10 mm) of diameter of the electrode with both samples sides, using an evaporation and substrate vacuum thermal system.

After electrode deposition process, copper wires constituted the electrodes by placing the wire on the aluminum electrode using silver paste, Then leave it to dry for (24 hours) for each side of the sample, that shown in figure (3-6).

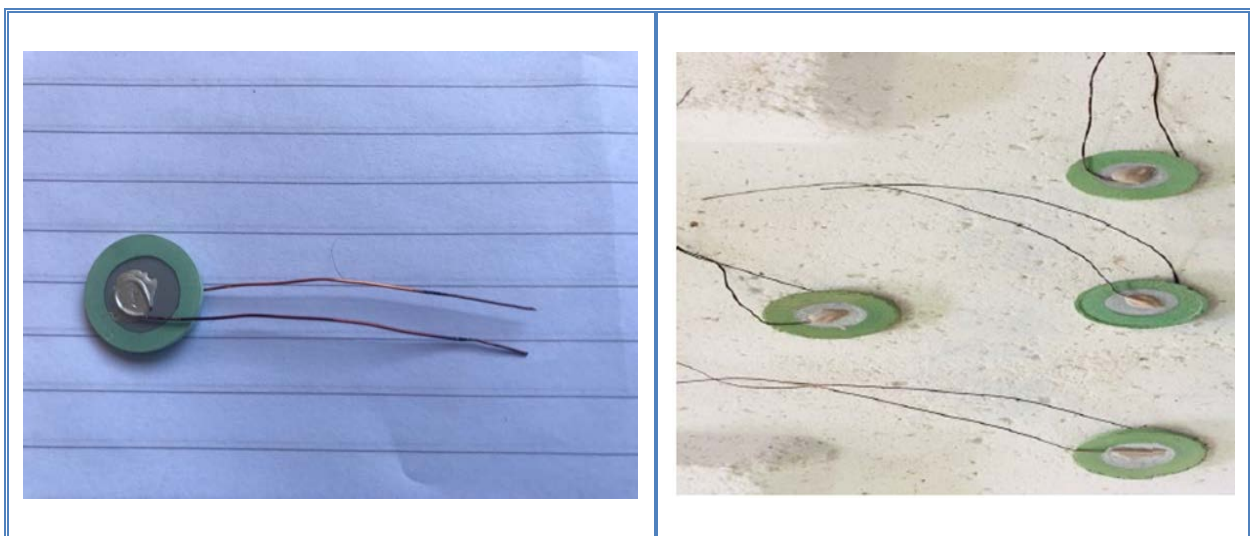


Figure (3-6) samples images after aluminum electrode

(3-3) X-Ray diffraction test

XRD test that used to distinguish the pure (Zinc Oxide and In_2O_3 nano powders) and discuss verify crystalline structure, lattice parameters and phase dissection for samples (BC/0 ,BC/1, BC/2 and BC/3) which sintered at three different temperatures (1000, 1050, 1100) °C .

XRD type source was (6000 Shimadzu), the functions include: {UK, Voltage: 40kV, Current: 30mA, Wavelength: 1.5406 Å} and continuous mode scans from (10° – 80°) of the samples.

(3-4) Measurement of electrical characteristics

The (I-V) measurement was calculated with using a homemade instrument, DC power supply (PHYWE, 0-10 KV, 2mA), Where the voltage during the tests altered manually, and two types of multimeters, were used; one as DC micrometer ($0.1 \mu A-20A$), and the other as a DC voltmeter (0.1mV-1000V), that shown in figure (3-7)

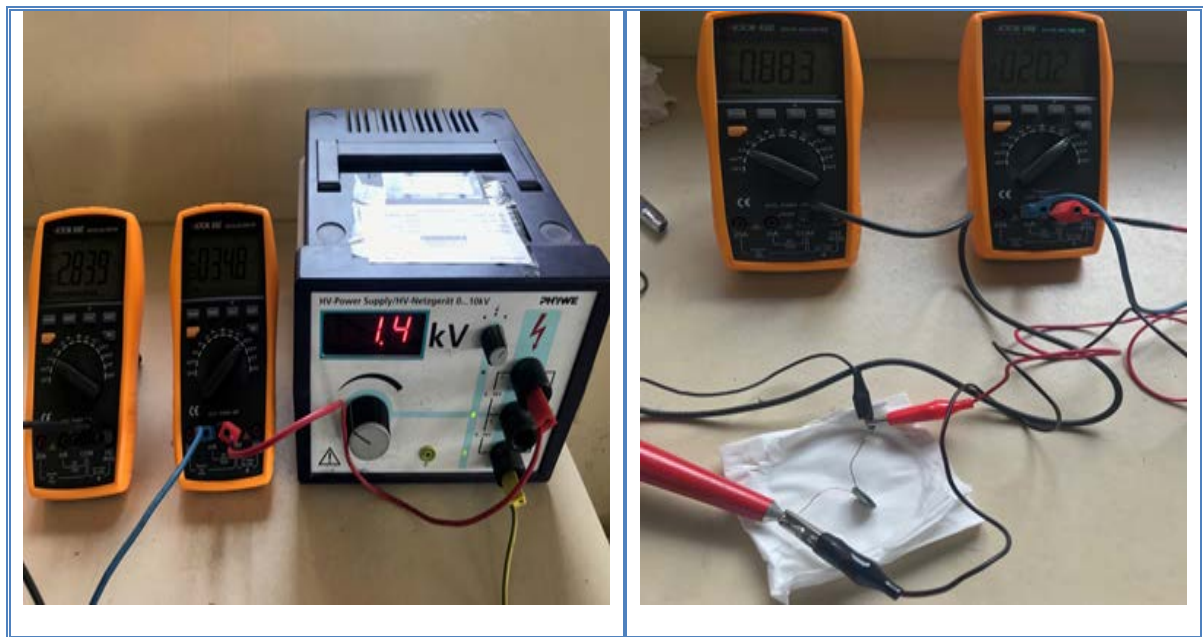


Figure (3-7) power supply and multimeters images

(3-4-1) Breakdown voltage (V_b)

Measure of voltage value ($V_{0.5 \text{ mA}}$) that is equivalent to (0.5mA) in contrast to the current value, and then calculate breakdown voltage values by using equation (2-12)

(3-4-2) Leakage current (I_L)

Calculate the present value in contrast to the ($V_{0.1}$ v) voltage value, and then calculate the leakage current values by using equation (2-10)

(3-4-3) Nonlinear coefficient (α)

The nonlinearity coefficient (α) can be calculated by using equation (2-9) after calculating the values of current and voltages.

(3-4-4) Dielectric features test

Dielectric features, such as the real dielectrical constant (ϵ') and the imaginary dielectric constant (ϵ'') {the loss factor ($\tan \delta$)} which investigated at (10 mV) in the range (5000Hz-1MHz), use the LCR meter that (LCR-8105G, 20 Hz - 5 MHz, RS-232,Taiwan) model which shown in the figure (3-8)



Figure (3-8) LCR meter image

(3-5) SEM test

To investigation of (In₂O₃) nano powder concentrations of dopants and the impact of sintering temperature on grain size that affecting on electrical characteristics, By scanning electron microscopy (SEM) the sintered ZnO samples with varying concentrations of indium oxide nano powder and various sintering temperatures were studied, type (INSPECT S50) at Technological university, as shown in figure (3-9).

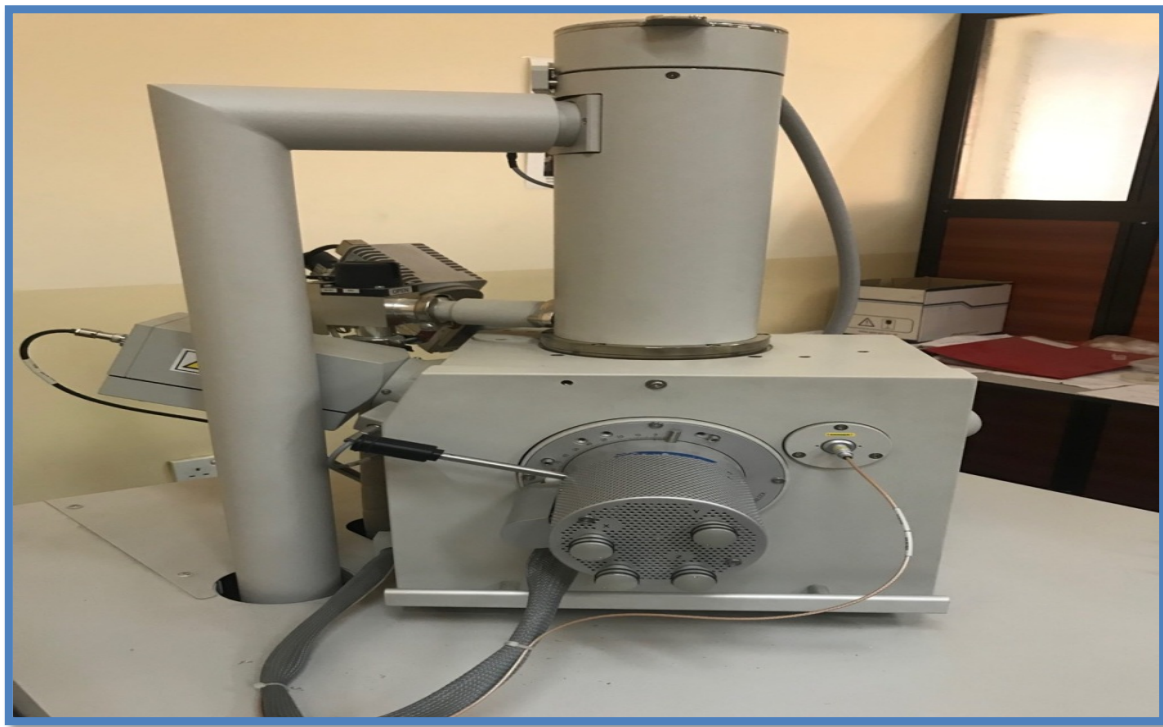


Figure (3-9) SEM device image

(3-6) I-V property measurement

The (I-V) current–voltage optical property mensuration was calculated with used the keithley Interactive Source Meter instrument model 2540, USA

With an external light source (tungsten) with a light intensity of about (1000 watts/meter) and spectrum about 300nm to 1.5mm, that shown in figure (3-10)



Figure (3-10) Interactive Source Meter with light source (tungsten)

CHAPTER FOUR

RESULTS AND DISCUSSION

(4-1) Introduction

I will discuss the results of the experimental study in this chapter and discuss the influence of sintering temperature and In_2O_3 nano powder dopant concentration on the changes in the ZnO-based crystal structure by varying tests and discusses, such as X-ray diffraction, Scanning electron microscopy, and the electrical properties with using some electrical tests like (breakdown voltage, nonlinear coefficient, leakage current, real dielectric constant, and loss factor) and optical properties like (I-V) optical properties.

(4-2) XRD results

We acquired a modality with many clear peaks by the XRD of Zinc oxide powder (raw material) at range of 2θ (20-70) degree concerning the plans.

That shown in figure (4-1). And when we contrasted the pattern observed with (WPDGT), it was comparable to the amount of the card (36-1461), (that shown in the appendix), that shown the powder is a hexagonal wurtzite polycrystalline – type structure.

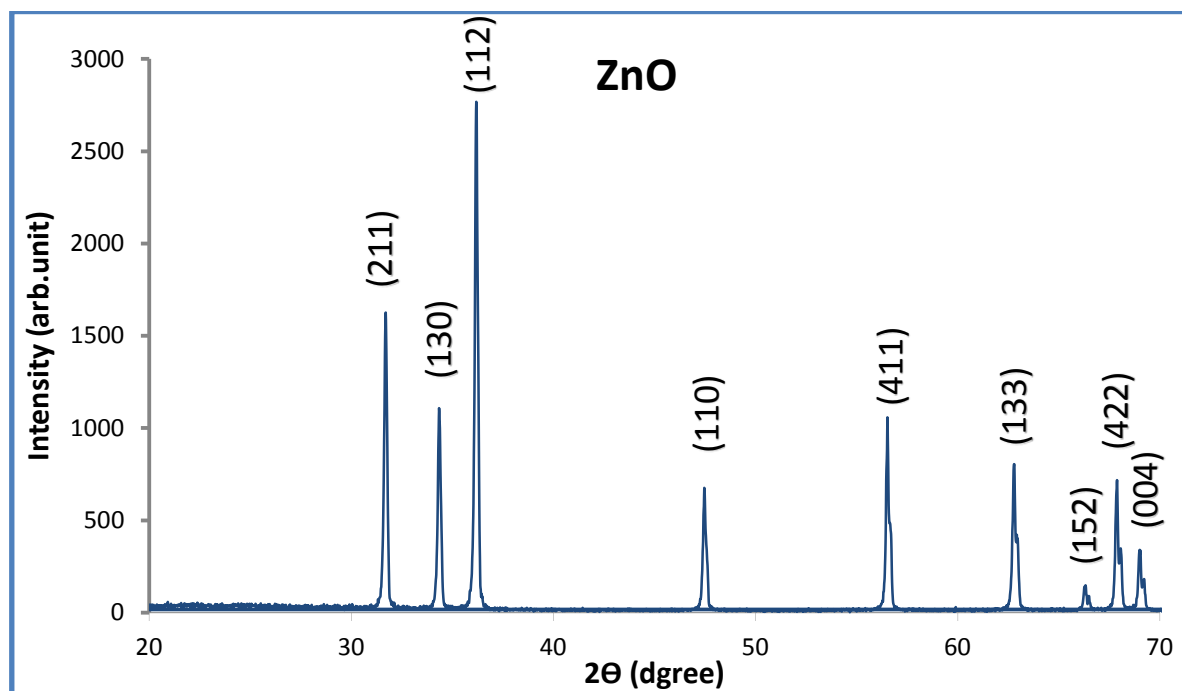


Figure (4-1) X-ray diffraction sketch for pure ZnO powder

As well the pure In_2O_3 nano powder XRD pattern shown in figure (4-2) which comparable with the card number pattern (06-0416) .This shows that the In_2O_3 powder used is cubic (that shown in the appendix)

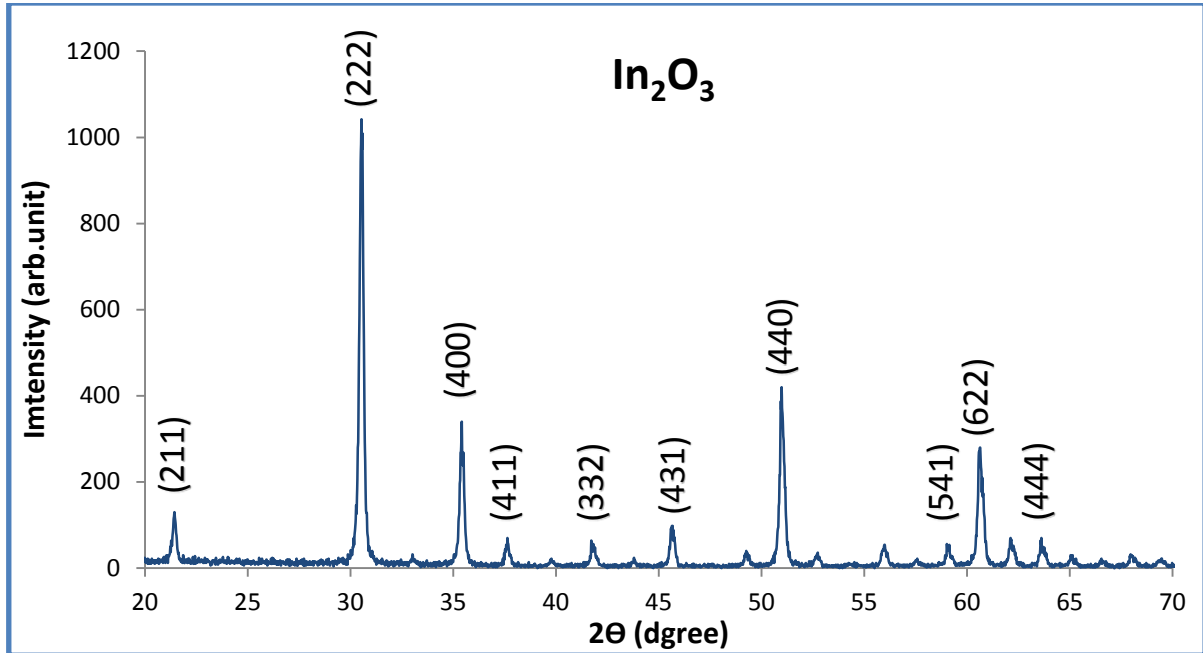


Figure (4-2) X-ray diffraction sketch for In_2O_3 nano powder

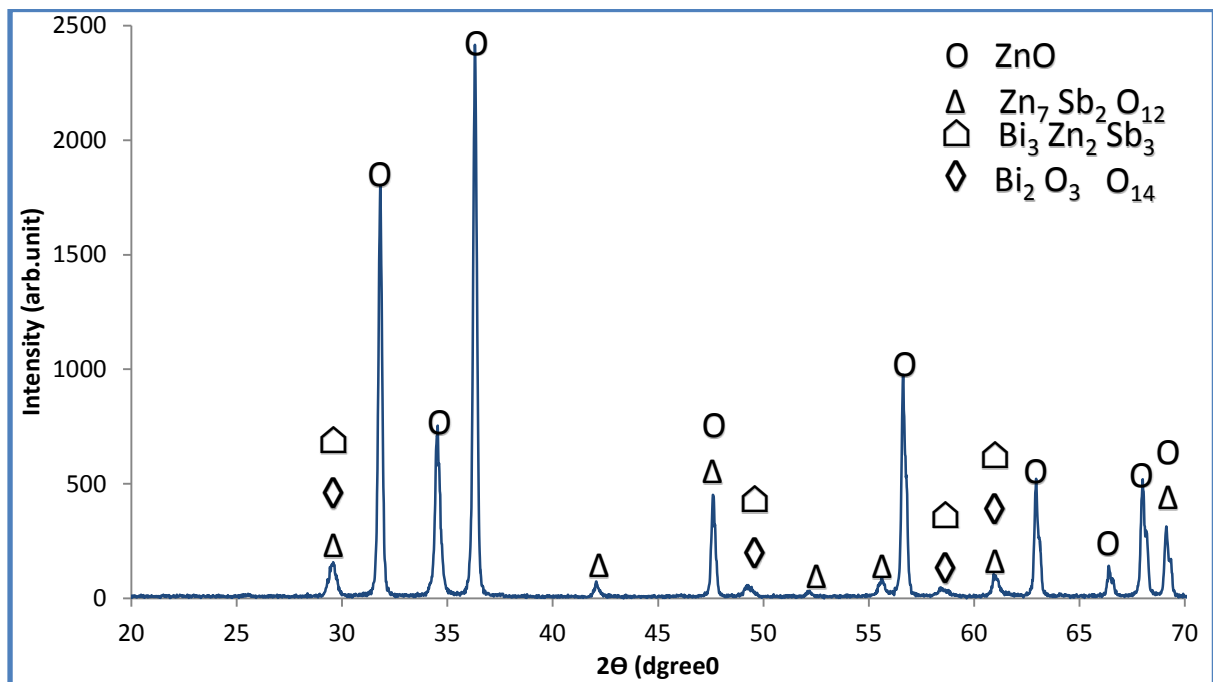


Figure (4-3) X-ray diffraction sketch for BC0 sample at 1000°C

From the (XRD) sample sketch (BC0) shown in figure (4-3), four phases can be seen there are : Zinc oxide phase, spinel phase, Pyrochlore phase and Bi-rich phase (Bi_2O_3) and that's in agreement with Shenghua Zhang work, (that shown in appendix) [19]

To investigate of the In_2O_3 nano powder influence as a dopant material on the Zinc oxide-based varistor's crystal structure, X-ray diffraction patterns are taken for specimens (BC1, BC2 and BC3) sintered at 1000°C and (BC3) for 1050°C and 1100°C .

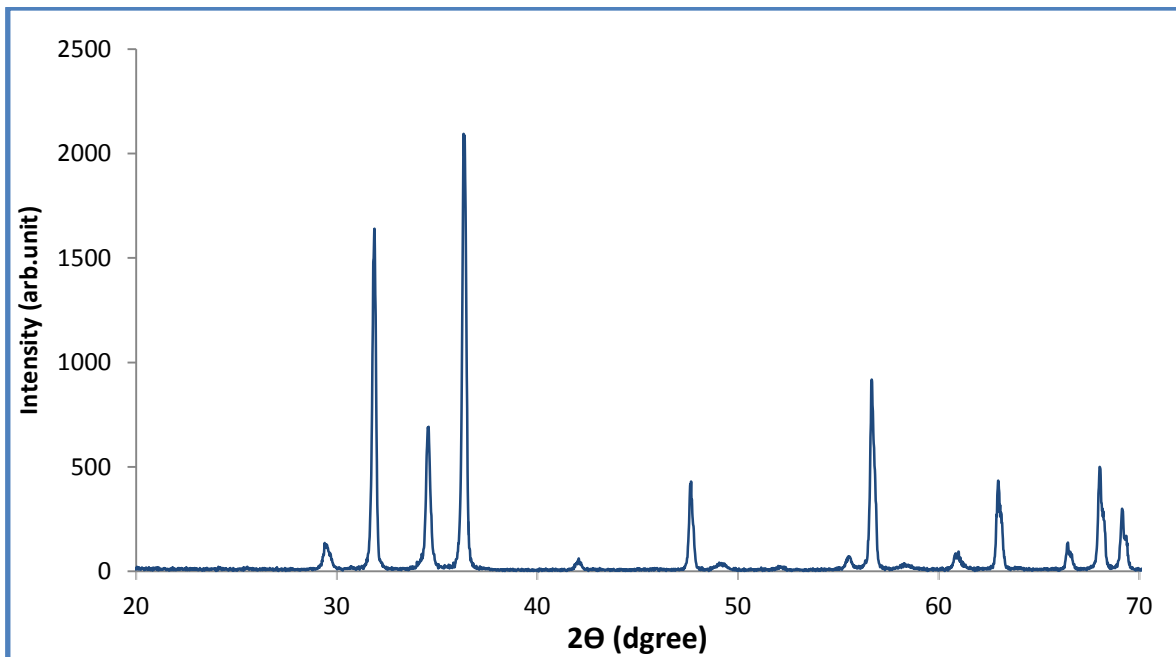


Figure (4-4) X-ray diffraction sketch for BC1 sample at 1000°C

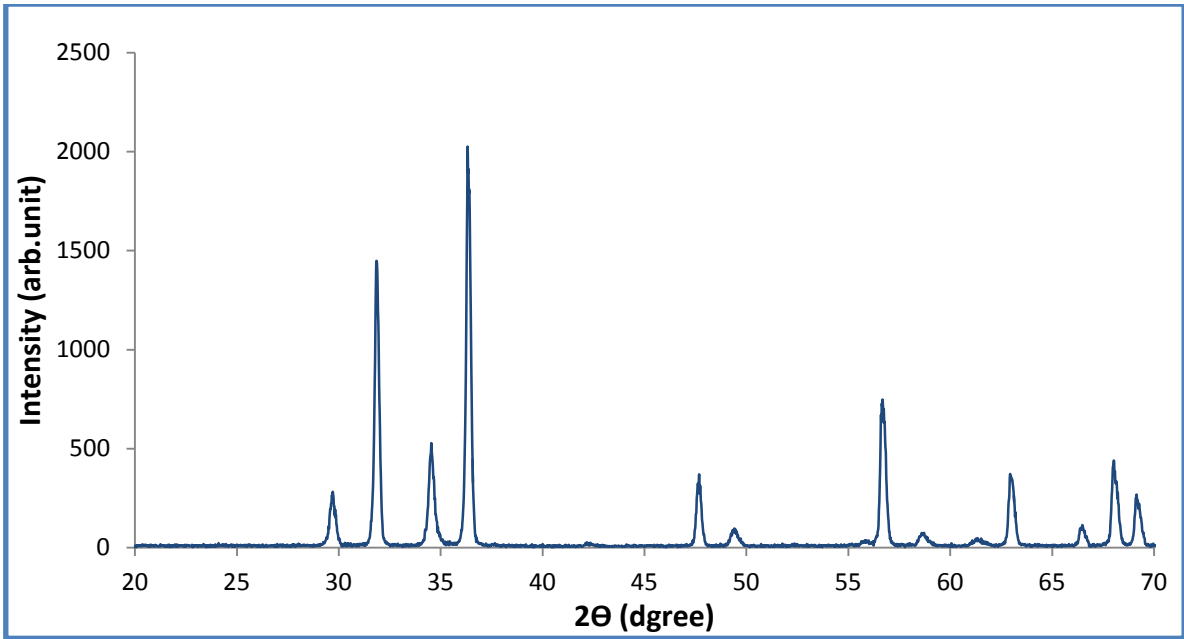


Figure (4-5) X-ray diffraction sketch for BC2 sample at 1000°C

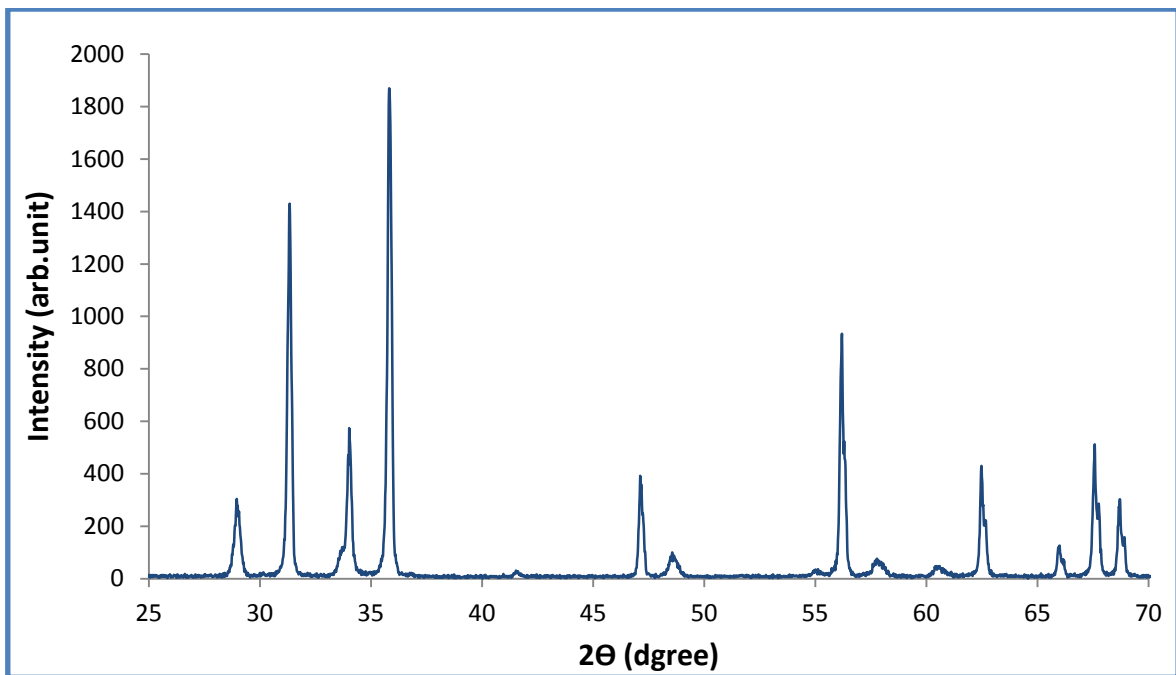


Figure (4-6) X-ray diffraction sketch for BC3 sample at 1000°C

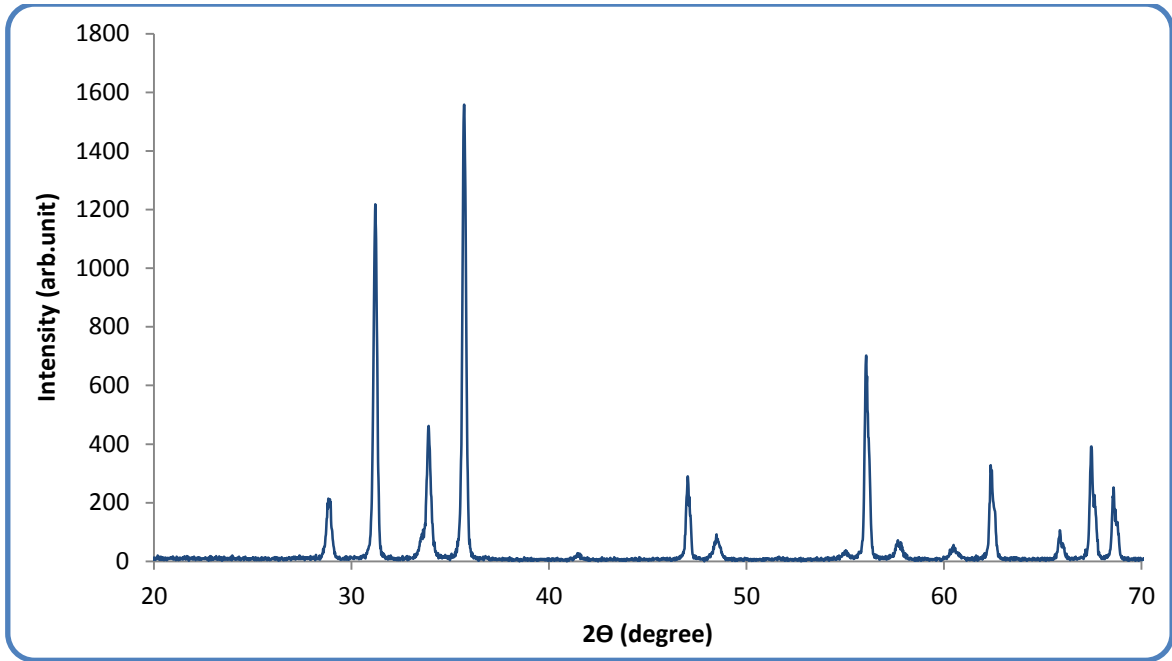


Figure (4-7) X-ray diffraction sketch for BC3 sample at 1050°C

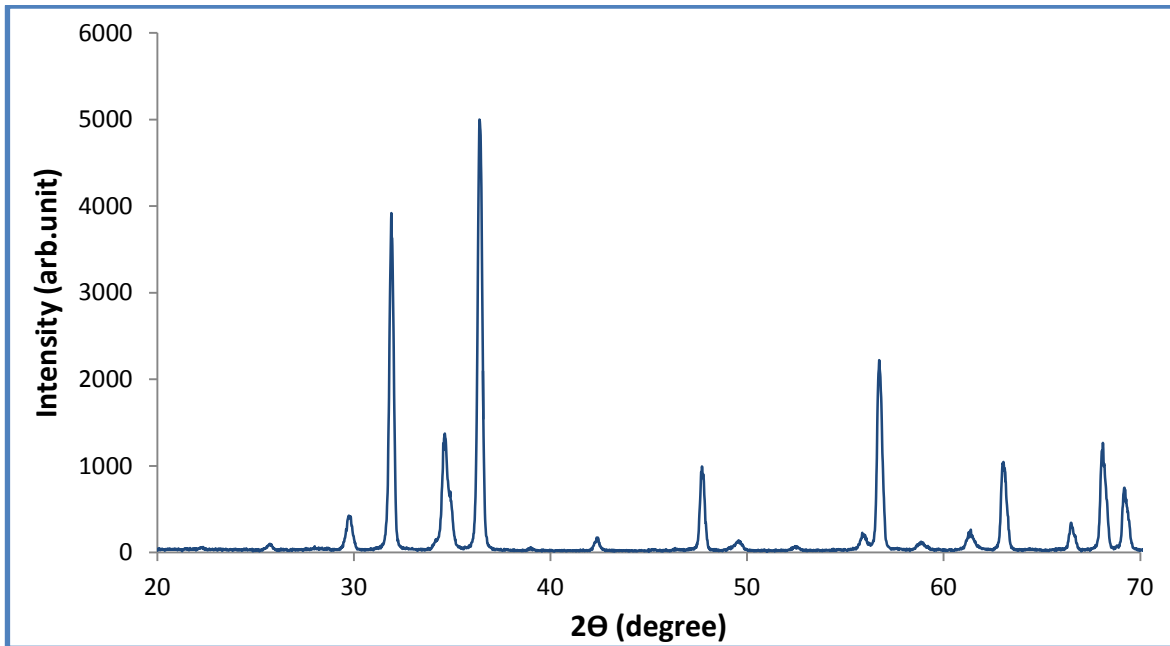


Figure (4-8) X-ray diffraction sketch for BC3 sample at 1100°C

In these XRD sketches for samples that sintered for 2 hours and shown in figures (4-4), (4-5) and (4-6) we can see that the peak intensity reduced with the increased concentration of In_2O_3 nano powder, this reduction in peak intensity could be attributed to that the dopant atom creates its own ZnO-lattice atomic

plans which produces XRD scattering not at the same phases, this leads to partial destructive interference this results in a reduction in peaks intensity [73].

The figures (4-6), (4-7) and (4-8) respectively for sample (BC3) at different sintering temperatures for 2 hours, we can see that with the increase in the sintering temperatures, the peak intensities are increased because of the influence of elevated temperatures on grain growth acceleration.

(4-3)The calculation of crystallite size:

The sample crystallite sizes in table (4-1) were calculated using the equation (2-15) of Deby-Scherrer with take the avarge of three strongest full Width (FWHM) and (2 theta) peaks values from the Xrd data process

Table (4-1) crystallite size of different samples with different sintering temperatures

| Samples | FWHM (degree) | 2θ (degree) | Diameter (nm) |
|-------------------|----------------------|--------------------------------------|----------------------|
| BC0 1000°C | 0.2143 | 41.2583 | 41.4295 |
| BC1 1000°C | 0.2689 | 40.9692 | 30.7054 |
| BC2 1000°C | 0.3466 | 40.9822 | 23.8220 |
| BC3 1000°C | 0.4077 | 40.9367 | 20.2519 |
| BC3 1050°C | 0.1993 | 41.6406 | 41.4295 |
| BC3 1100°C | 0.1828 | 41.5989 | 45.1682 |

Table (4-1) shows that the size of crystallite reduces as the concentration of In_2O_3 nano powder increases, this reason due to the formation of a spinal phase (ZnIn_2O_4) by (In_2O_3) that plays a major role in inhibiting grain growth, and this agree with [32]

From the table (4-1) we can see the elevation in crystallite sizes with the elevated of sintering temperature, on sample BC3 sintered at (1100°C) it arrives (45.1682 nm). This is because of the influence of elevated sintering temperatures on the growth of grains [67]

(4-4) SEM test

The (SEM) scans the sintered sample surface (BC0 and BC3) at (1000°C) for 2hours as well as the sintered (BC3) samples at (1050 and 1100) $^\circ\text{C}$ for 2 hours. As shown in figure (4-9)

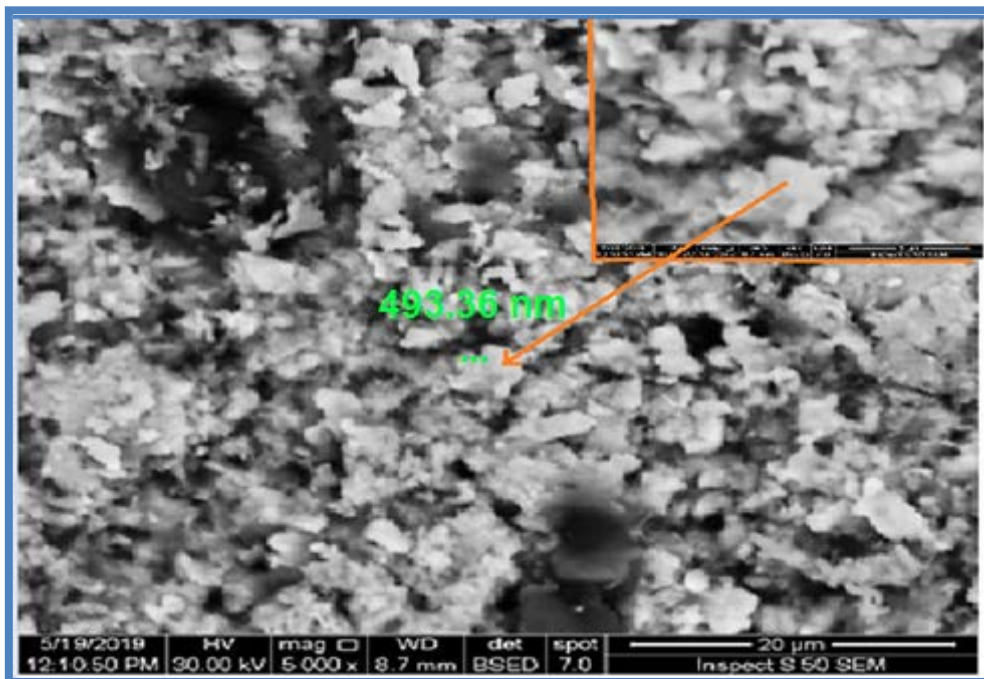


Figure (4-9-a) SEM image for pure (BC0) sample sintered at (1000°C)

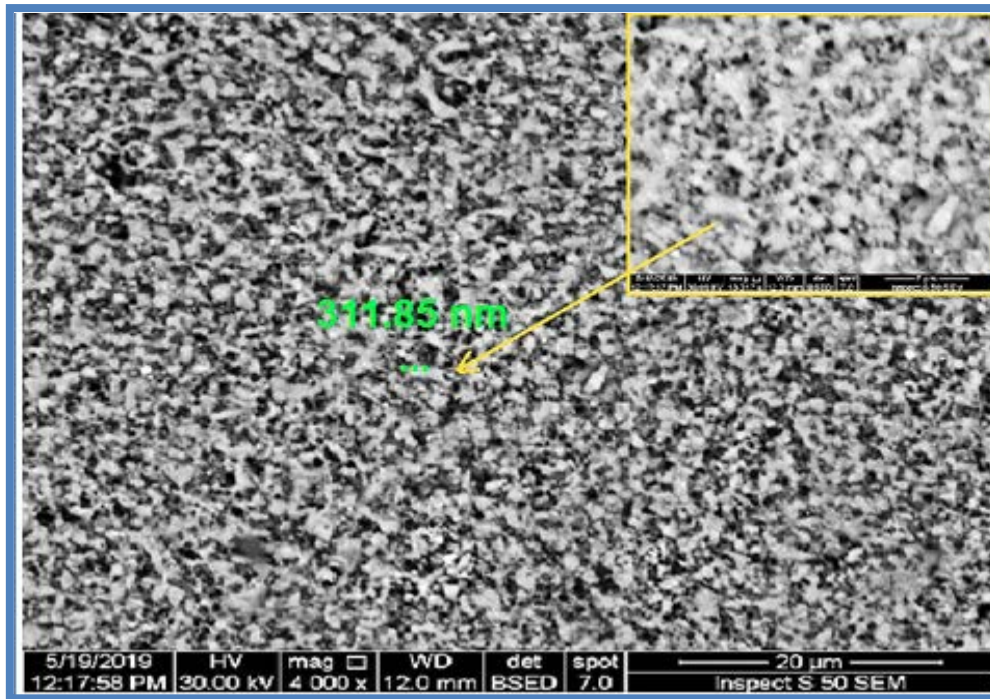


Figure (4-9-b) SEM image for (BC3) sample sintered at (1000) °C

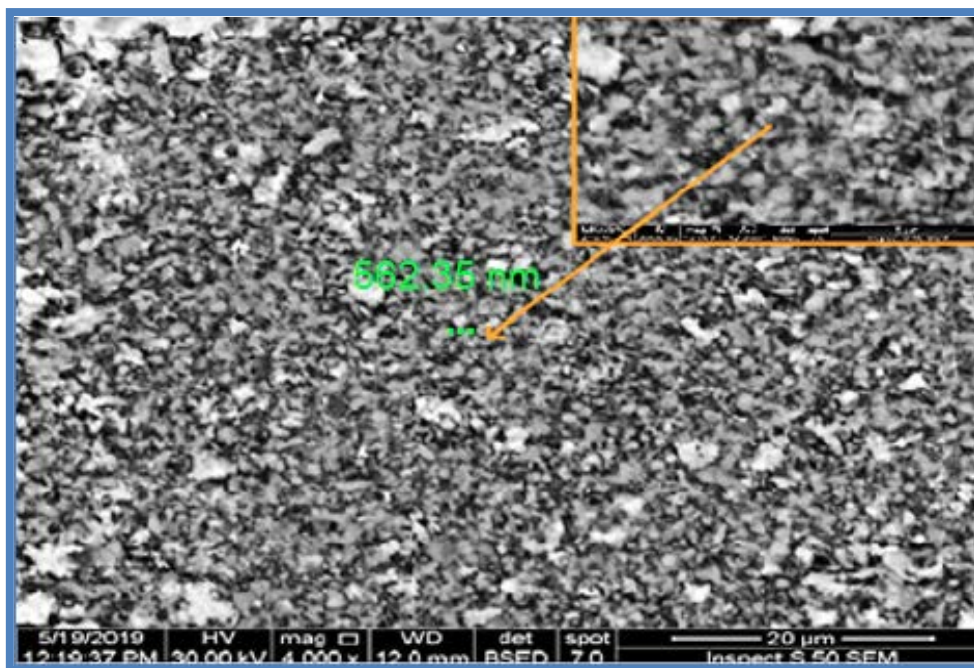


Figure (4-9-c) SEM image for (BC3) sample sintered at (1050) °C

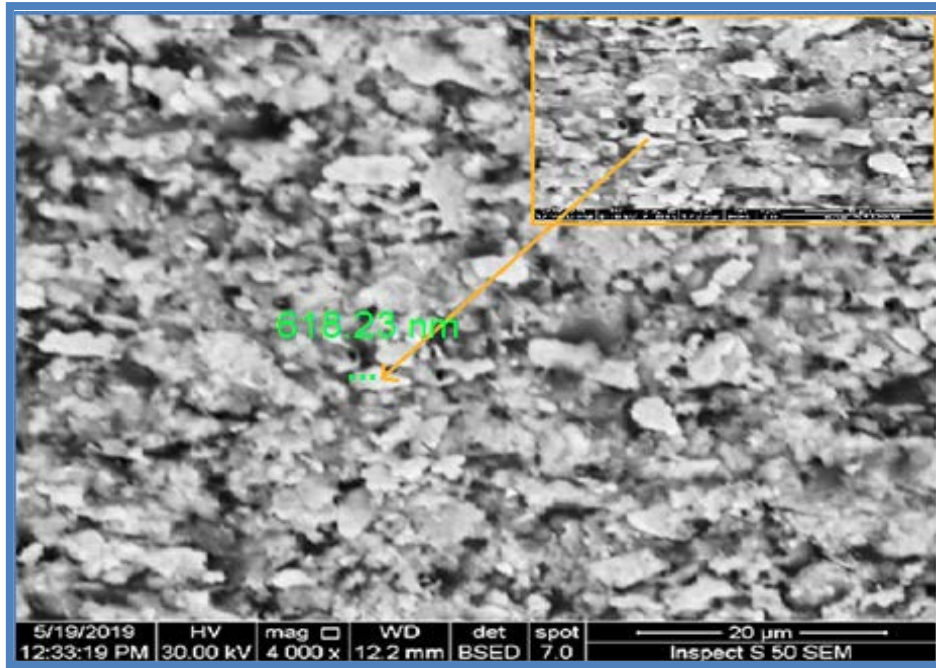


Figure (4-9-d) SEM image for (BC3) sample sintered at (1100) °C

Table (4-2) shows the diameter of some grains of the samples, wicth determined by SEM

| Samples | Diameter (nm) |
|-------------------|----------------------|
| BC0 1000°C | 493.36 |
| BC3 1000°C | 311.85 |
| BC3 1050°C | 562.35 |
| BC3 1100°C | 618.23 |

We have the ability to see the average diameter decreased partially as the concentration of nanoic (In_2O_3) increases, this is due to the In_2O_3 nano powder mixing composed a spinel phase that decreases the ZnO grain boundaries growth, causes grain size decreases, and that's in agreement with work [60]

The average diameter of the grains were significantly increased with elevated of sintering temperature, the higher sintering temperature speeds up the growth of ZnO grain, that agree with [21].

(4-5) The electrical mensuration:

(4-5-1) Breakdown voltage (V_b)

The (V_b) of any varistor sample was calculated when a current of (0.5mA) Passed through the circuit-connected varistor. The (V_b) values for the samples are shown in the table (4-3) that we can notice the increases of (V_b) with evaluate the In_2O_3 nano powder concentration at different sintering temperature, which evaluated from (1287V) for BC0 sample to (2080V) for BC3 sample, which they sintered at (1000°C) for 2h.

That increase of (V_b) can be ascribed to the In_2O_3 nano powder forming spinel phase (ZnIn_2O_4) inhibiting the growth of grain by locating the grain boundaries lead to increaase the amount of grain boundaries and then rise the (V_b) values of the varistor, depending on the equation (2-12), and that's agree with Maura Kelleher [55].

Table (4-3) the measured of (V_b) of the samples

| Samples | The breakdown Voltage(v_b) (v) |
|-------------------|--|
| BC0 1000°C | 1287 |
| BC1 1000°C | 1600 |
| BC2 1000°C | 1840 |
| BC3 1000°C | 2080 |
| BC0 1050°C | 1096 |
| BC1 1050°C | 1240 |
| BC2 1050°C | 1085 |
| BC3 1050°C | 1360 |
| BC0 1100°C | 1043 |
| BC1 1100°C | 1126 |
| BC2 1100°C | 1096 |
| BC3 1100°C | 1188 |

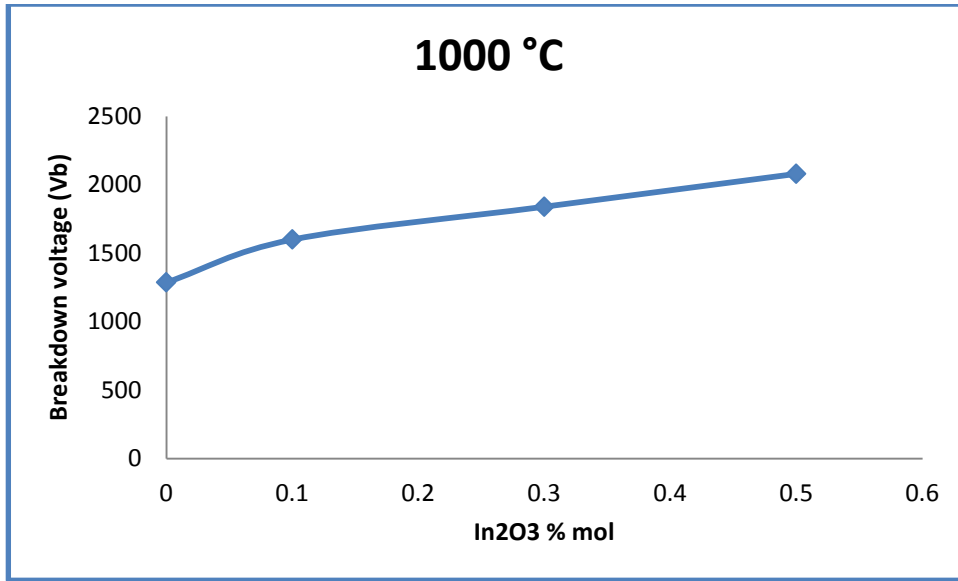


Figure (4-10) divergence of breakdown voltage with increased In₂O₃ % mol concentration at 1000°C

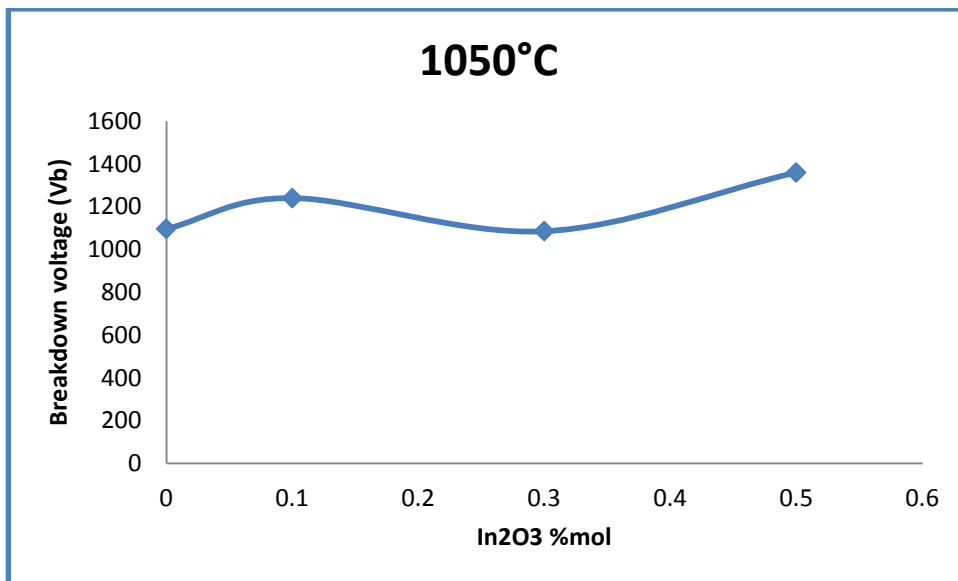


Figure (4-11) divergence of breakdown voltage with increased In₂O₃ % mol concentration at 1050°C

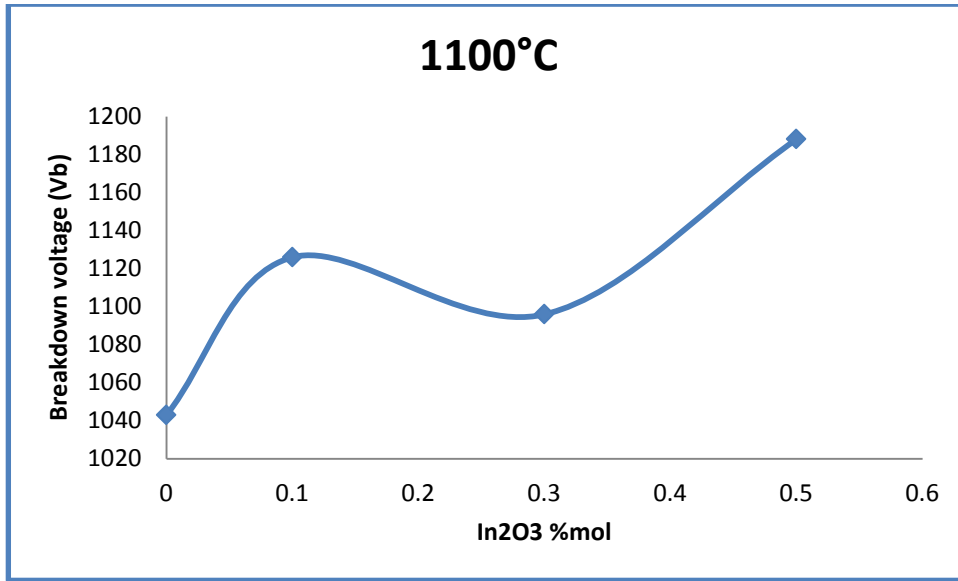


Figure (4-12) divergence of breakdown voltage with increased In₂O₃ % mol concentration at 1100°C

It is possible for us to note that (V_b) decreased as sintering temperature increased at certain concentrations of In₂O₃ nano powder so for example it was declining from (2080V) to (1188V) for BC3 sample at the temperature of sintering increases from 1000°C to 1100°C. This sharp reduction because of the rise in grain growth as a cursor of sintering temperature that decreases the amount of grain boundaries.

(4-5-2) leakage current (I_L)

(I_L) was calculated when the voltage from the breakdown voltage was equal to (0.8), that shown in the table (4-4)

Table (4-4) leakage current measurements for all samples

| Samples | Leakage Current (mA) |
|-------------------|-----------------------------|
| BC0 1000°C | 0.21 |
| BC1 1000°C | 0.14 |
| BC2 1000°C | 0,02 |
| BC3 1000°C | 0.03 |
| BC0 1050°C | 0.27 |
| BC1 1050°C | 0.09 |
| BC2 1050°C | 0.04 |
| BC3 1050°C | 0.01 |
| BC0 1100°C | 0.34 |
| BC1 1100°C | 0.28 |
| BC2 1100°C | 0.18 |
| BC0 1000°C | 0.13 |

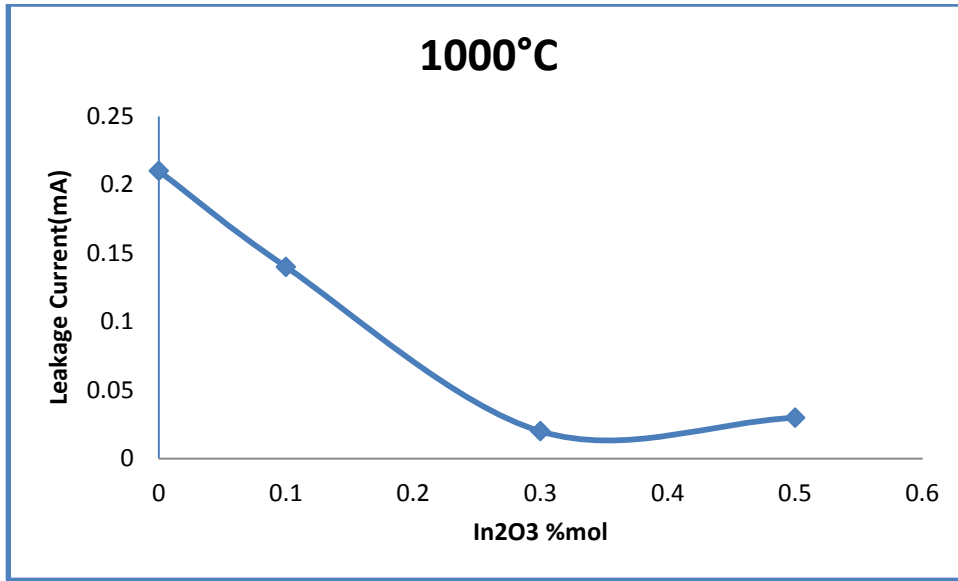


Figure (4-13) divergence of the leakage current with increased In₂O₃ % mol concentration at 1000°C

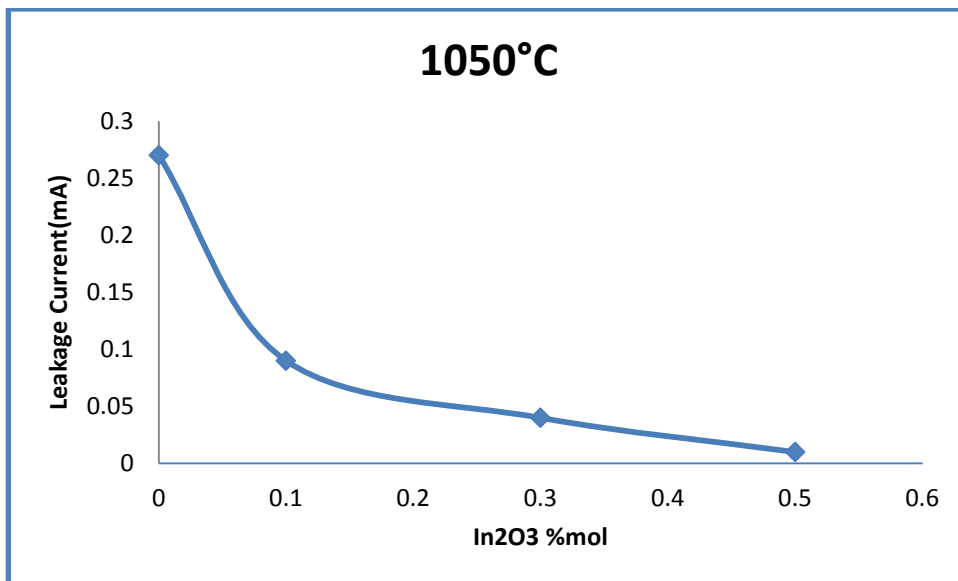


Figure (4-14) divergence of the leakage current with increased In₂O₃ % mol concentration at 1050°C

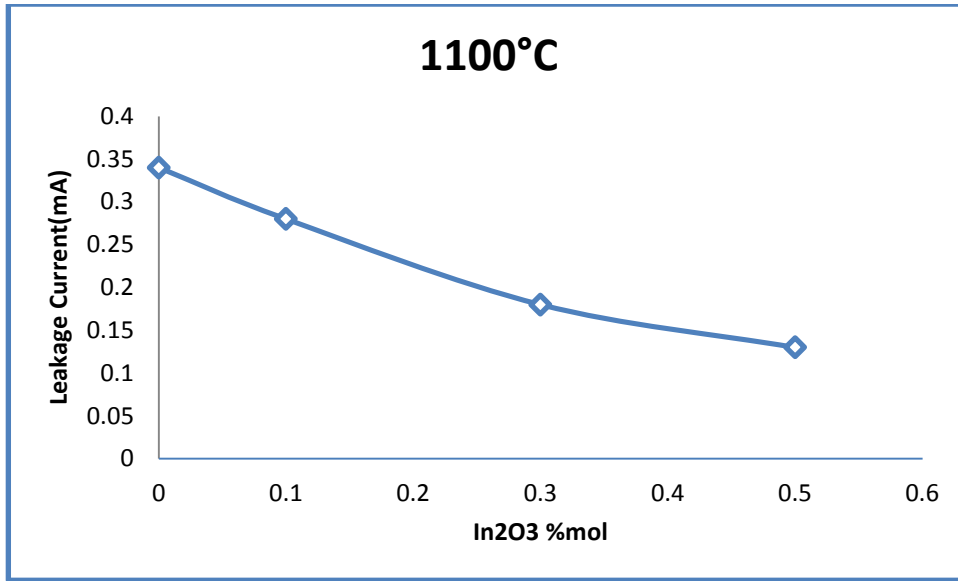


Figure (4-15) divergence of the leakage current with increased In₂O₃ % mol concentration at 1100°C

From table (4-4) and figures (4-13), (4-14) and (4-15) we can see that the current of leakage decreased with the increase of In₂O₃ nano powder at every situation of sintering, the decrease in the current of leakage may be due to that In₂O₃ nano powder will increase the area of attrition layer, when this layer is increased, the charge carriers are unable to cross the charge and then reduce the leakage current, that agree with [59].

And we can be observed that the current of leakage rises as the sintering temperature rises, due to that Indium dopants function as a granter in Zinc oxide lattice, so that the conductive band charge carrier raises ZnO grain resistance, and that increases the leakage current.

This can be attributed to the addition of insoluble (Bi₂O₃) in ZnO and the grain boundaries make a highly charged layer and raise the interface resistance resulting in a higher (v_b) and a reduction in the leakage current value, that is agree with [8]

(4-5-3) The nonlinear coefficient (α)

The non-linear coefficient (α) is the extreme significant parameter in varistor work and constitutes the highest criterion parameter among other varistor parameters or characteristics. The nonlinear coefficient for all the samples was determined using equation (2-9), and displayed in the table (4-5).

Table (4-5) nonlinear coefficient values for all samples

| Samples | Nonlinear coefficient (α) |
|-------------------|--|
| BC0 1000°C | 15.87 |
| BC1 1000°C | 35.71 |
| BC2 1000°C | 37.03 |
| BC3 1000°C | 39.17 |
| BC0 1050°C | 10.98 |
| BC1 1050°C | 25.29 |
| BC2 1050°C | 28.11 |
| BC3 1050°C | 38.32 |
| BC0 1100°C | 12.52 |
| BC1 1100°C | 13.33 |
| BC2 1100°C | 19.41 |
| BC3 1100°C | 30.30 |

The measurements of I-V properties tests were done for samples (BC0, BC, BC2 and BC3) sintered at three different temperatures, and we can observe nonlinear behavior in these curves, that shown in following figures.

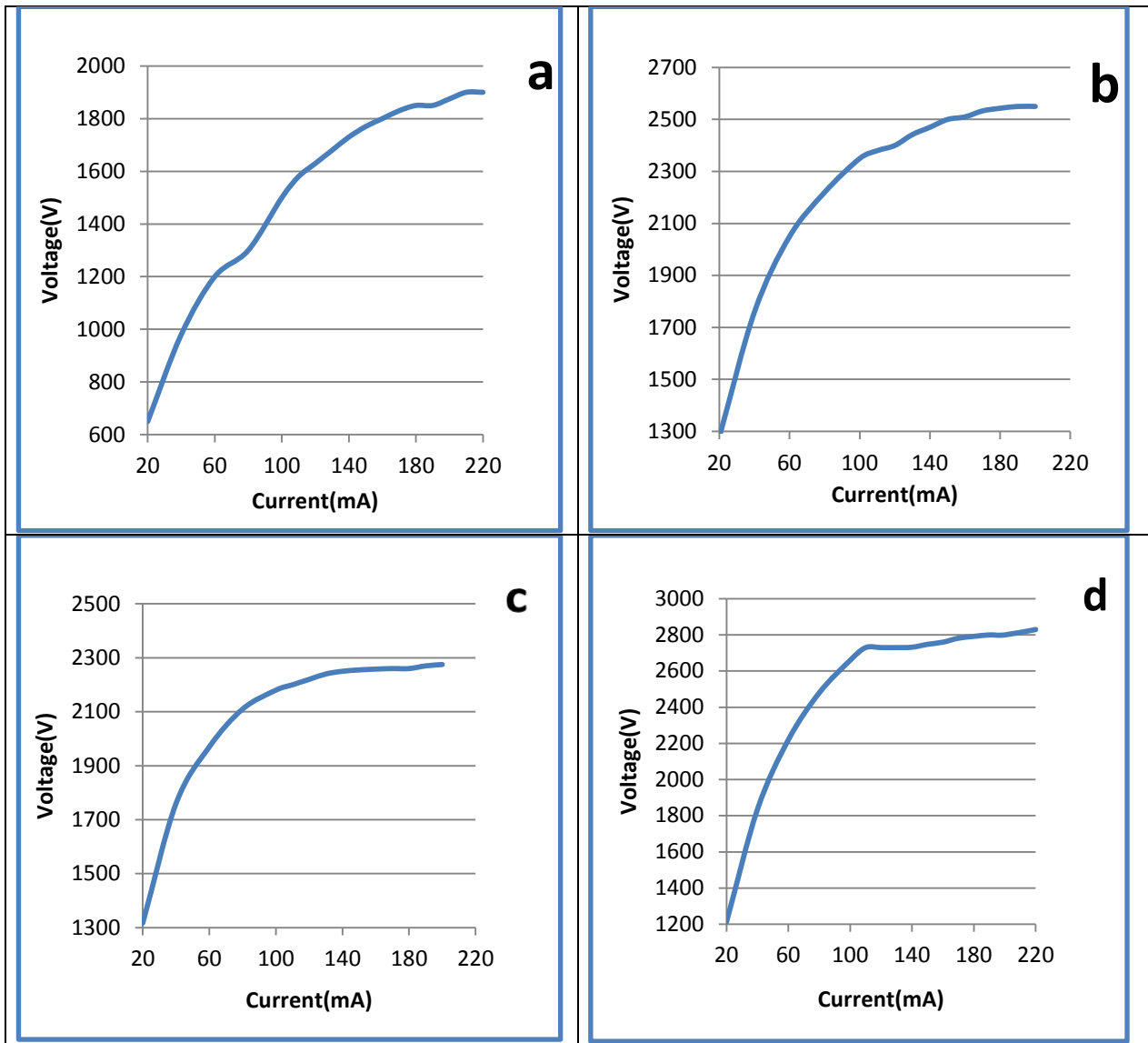


Figure (4-16) I-V curve for:

- a) BC0 1000°C sample, b) BC1 1000°C sample**
c) BC2 1000°C sample, d) BC3 1000°C sample

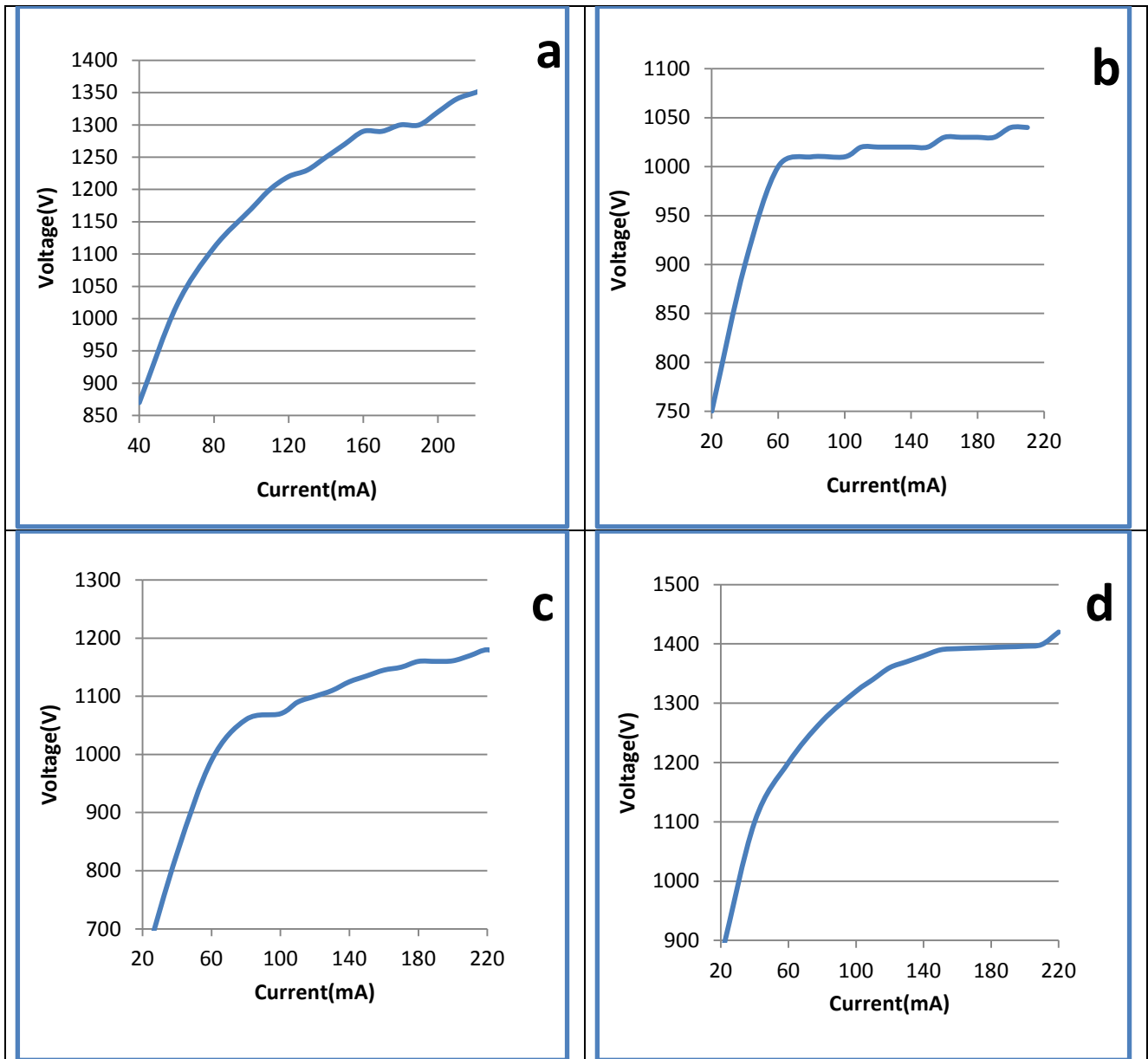


Figure (4-17) I-V curve for:

a) BC0 1050°C sample, b) BC1 1050°C sample

c) BC2 1050°C sample, d) BC3 1050°C sample

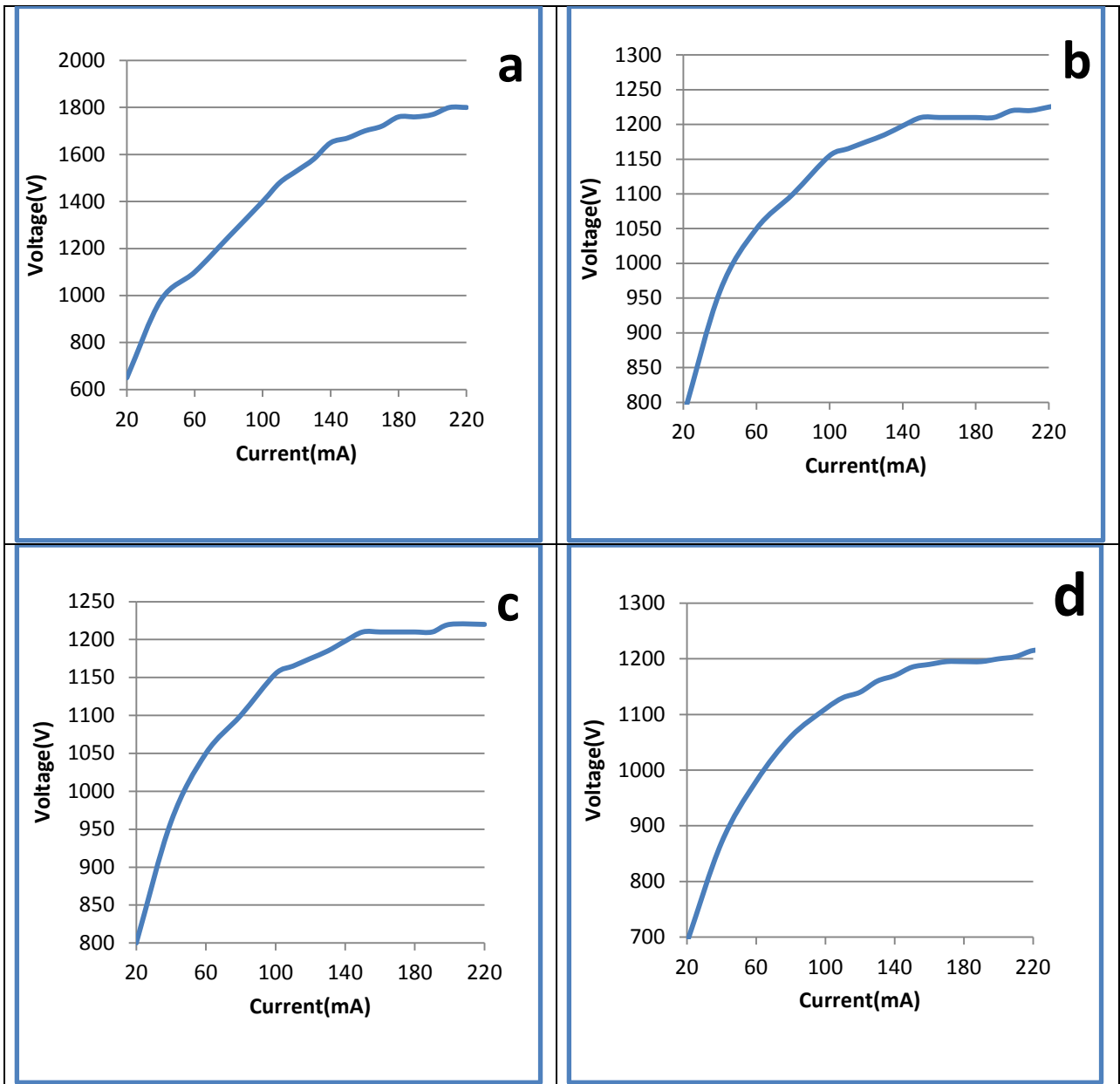


Figure (4-18) I-V curve for:

a) BC0 1100°C sample, b) BC1 1100°C sample

c) BC2 1100°C sample, d) BC3 1100°C sample

From the values of the table (4-5) and figures (4-16), (4-17) and (4-18) we can note the increasing of nonlinear coefficient gradually with increasing In_2O_3 nano powder doping and other oxides, so we notice that the nonlinear coefficient values of the samples BC3, BC2 and BC1 clearly improved gradually relative to the BC0 samples. This increase is due to nonlinearity behavior owing to the addition of oxide dopants and the fact that In_2O_3 nano powder inoculation leads to the increase and regularity of the formation of Schottky barriers between grain boundaries, that is agree with [74]

And decrease of nonlinear coefficient with evaluating the sintering temperatures. This decrease in (α) is due to the increase in sintered temperature lead to increases the grains growth and reduce the Schottky barriers, which leads to reduce the coefficient of nonlinearity , reported by [75].

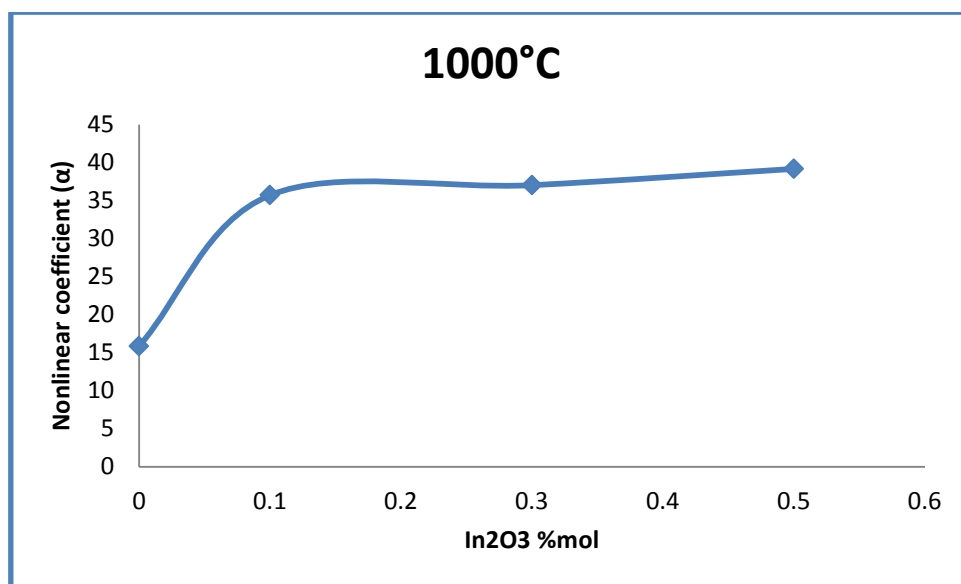


Figure (4-19) divergence of the nonlinear coefficient with increased In_2O_3 % mol concentration at 1000°C

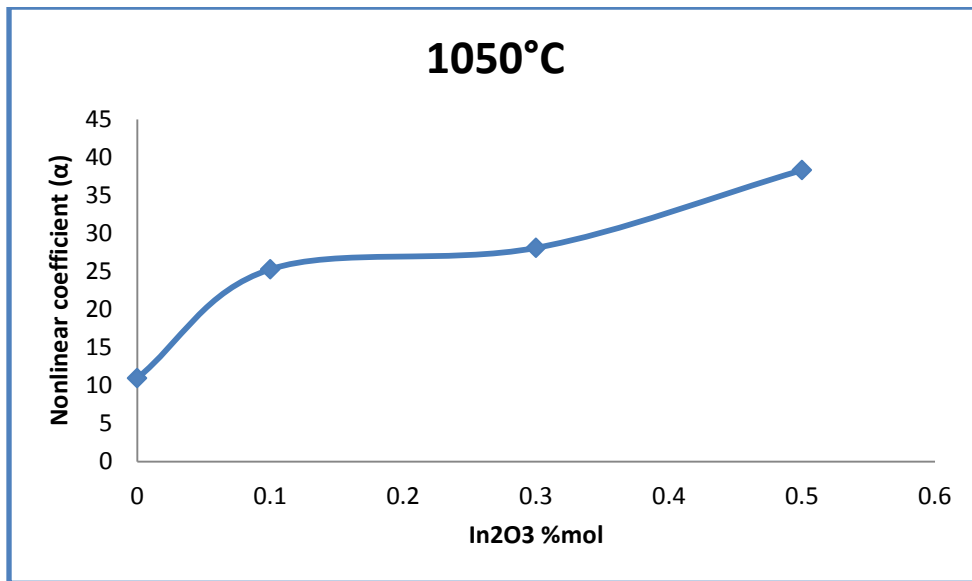


Figure (4-20) divergence of the nonlinear coefficient with increased In₂O₃ % mol concentration at 1050°C

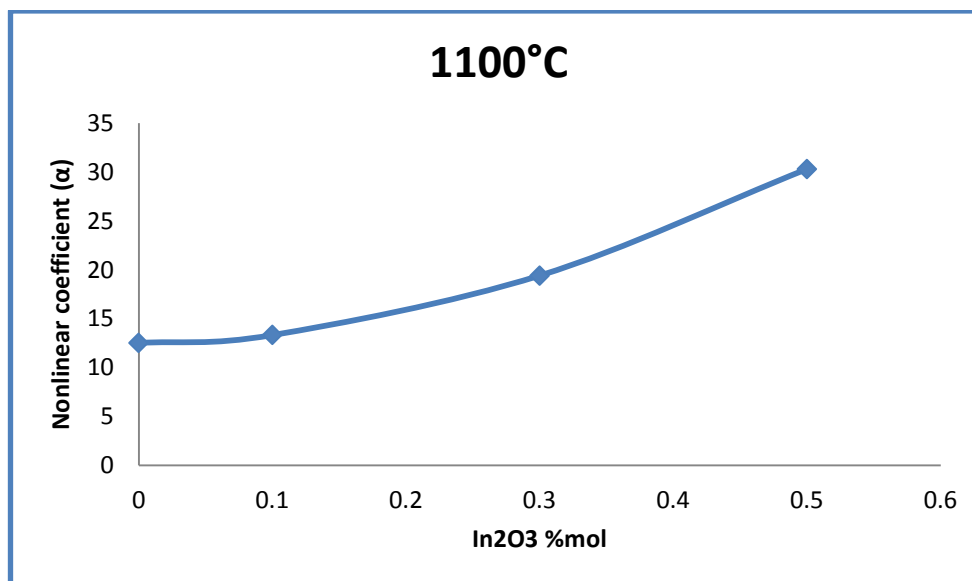


Figure (4-21) divergence of the nonlinear coefficient with increased In₂O₃ % mol concentration at 1100°C

(4-5-4) Dielectric constant (ϵ')

To study the effect on the dielectric constant of the In_2O_3 nano powder concentration and sintering temperature, the dielectric constant was measured for samples (BC0, BC1, BC2, BC3) which were all sintered at 1050°C , and for samples (BC1, BC3) which sintered at 1100°C . With frequency range at room temperature (500Hz-1MHz).

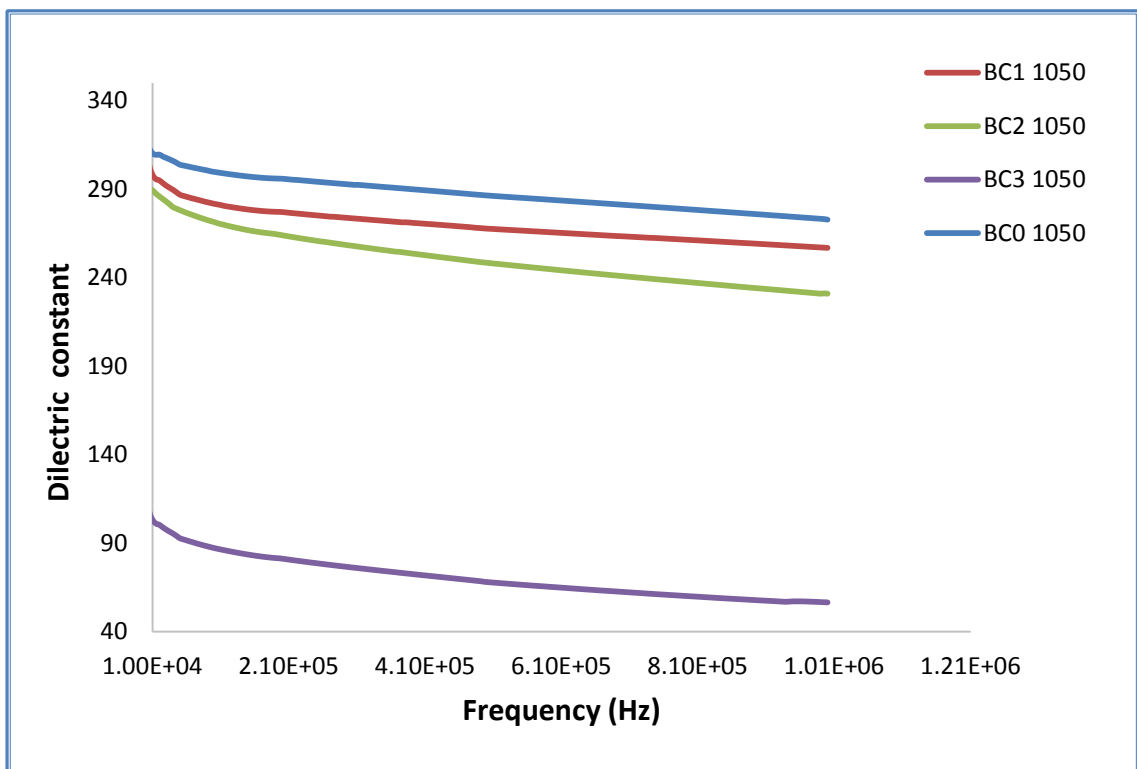


Figure (4-22) Dielectric constant for (BC0, BC1, BC2 and BC3) as a frequency function sintered at 1050°C

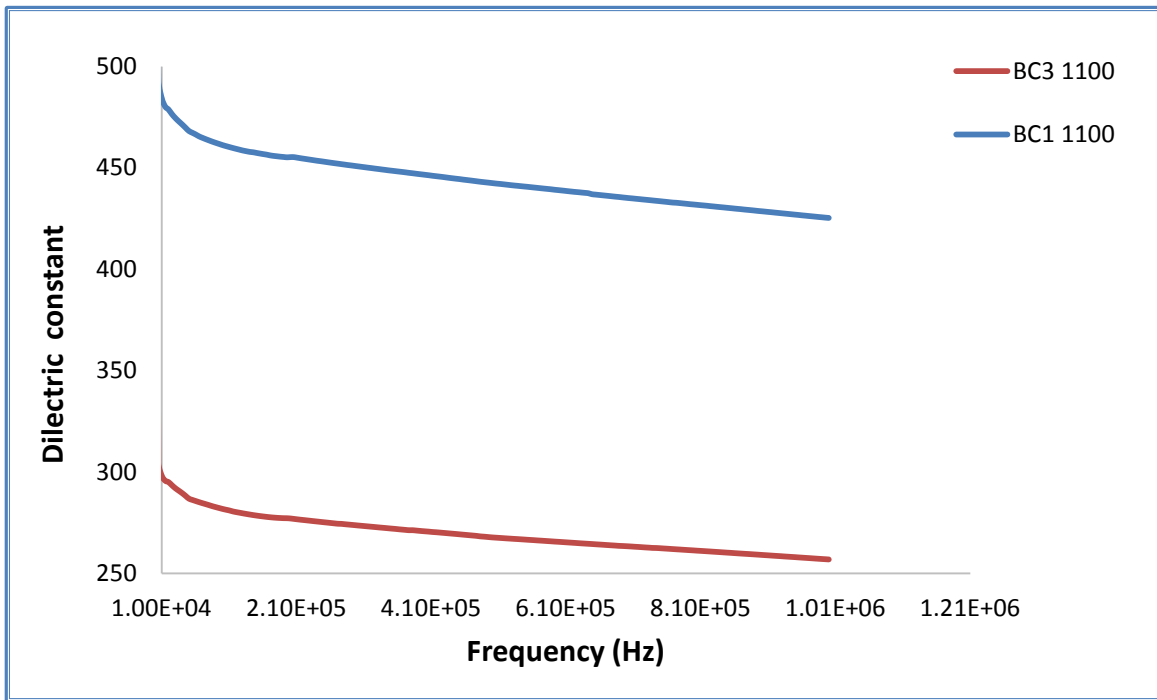


Figure (4-23) Dielectric constant for (BC1 and BC3) as a frequency function sintered at 1100°C

From above figures the decrease in dielectric constant can be seen with the increase in sample frequency, this decrease can be attributed to when the frequencies increase, the dipoles are unable to keep up with these frequencies, the vibration increases and the direction of the electrical field is very rapidly reflected, which decreases polarization and decreases static isolation. [76]

We can also notice that the samples sintered at higher temperatures have a high constant dielectric value, this is due to the bigger size of ZnO grain and reduced grain boundaries of the samples and that's the same reason why dielectric constant decreases with the evaluated in concentricity nanoic (In_2O_3) inhibiting grain growth [77].

(4-5-5) Dissipation factor (loss factor):

The loss factor was measured for samples (BC0, BC1, BC2 and BC3) all sintered at 1050°C and for samples (BC1, BC3) sintered at 1100°C to study the influence on the loss factor of the In_2O_3 nano powder concentration and sintering temperature as a frequency function.

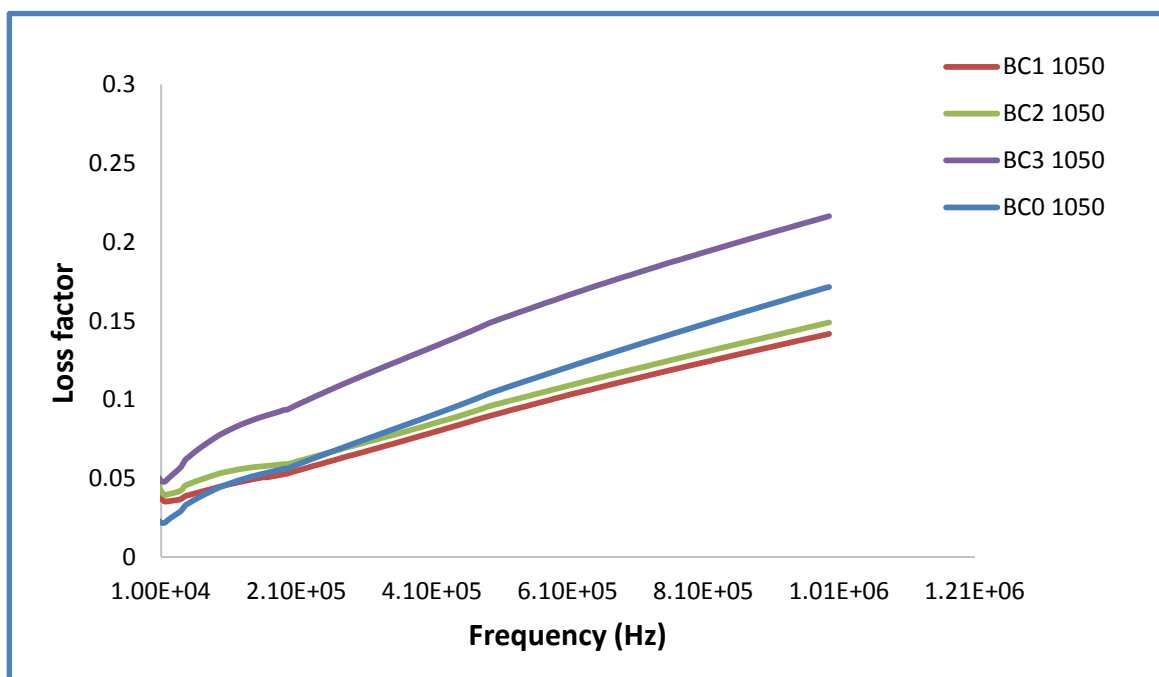


Figure (4-24) loss factor for (BC0, BC1, BC2 and BC3) as a frequency function sintered at 1050°C

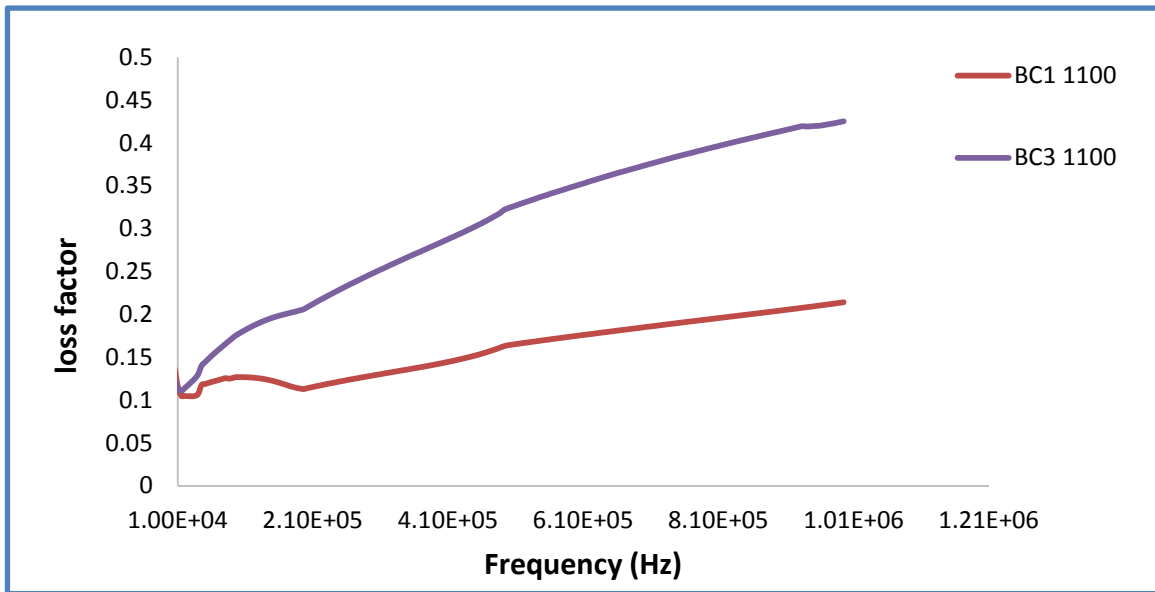


Figure (4-25) loss factor for (BC1 and BC3) as a frequency function sintered at 1100°C

From (4-24) and (4-25) figures we can see that the loss factor increase with increasing the concentration of In_2O_3 nano powder significantly higher loss factor due to increased sintering temperature with higher In_2O_3 nano powder concentration this is because of the presence of In_2O_3 , which leads to increase the energy loss as the leakage current [78].

(4-6) I-V properties measurements:

In order to study the effect of the intensity of the fallen radiation on the samples as well as the effect of darkness on I-V properties, the tests were done for samples (BC0, BC3) sintered at 1000°C and (BC3) samples that sintered at 1050°C and 1100°C, the results were shown in the figures:

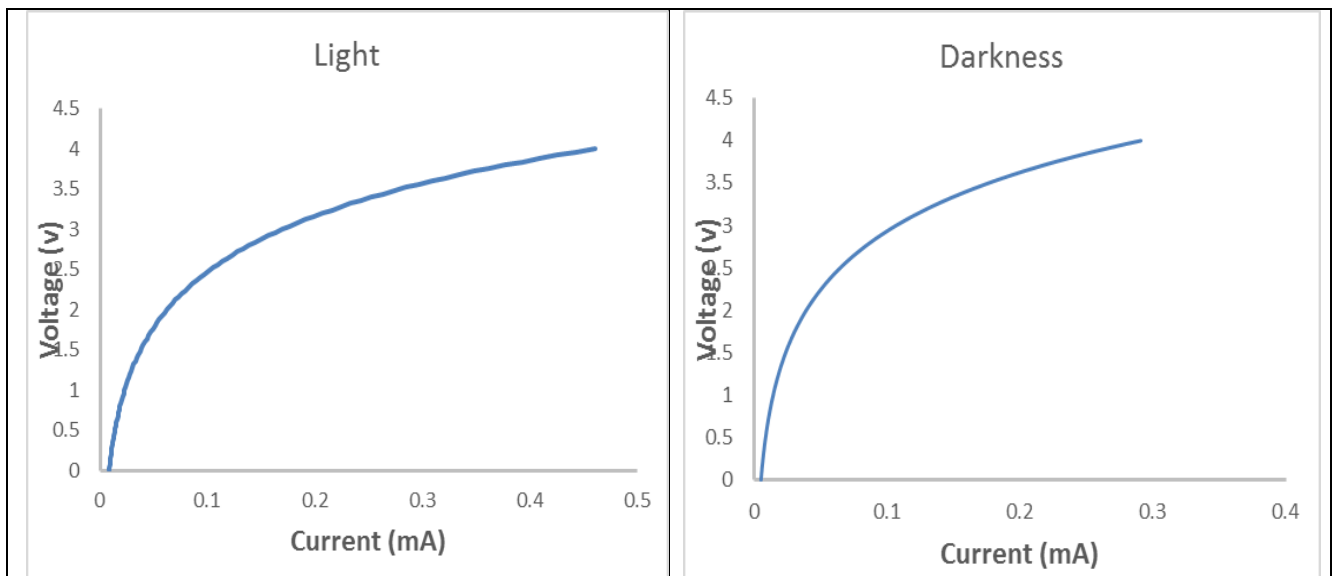


Figure (4-26) I-V test curve for 1000°C sample (BC0) at light and darkness

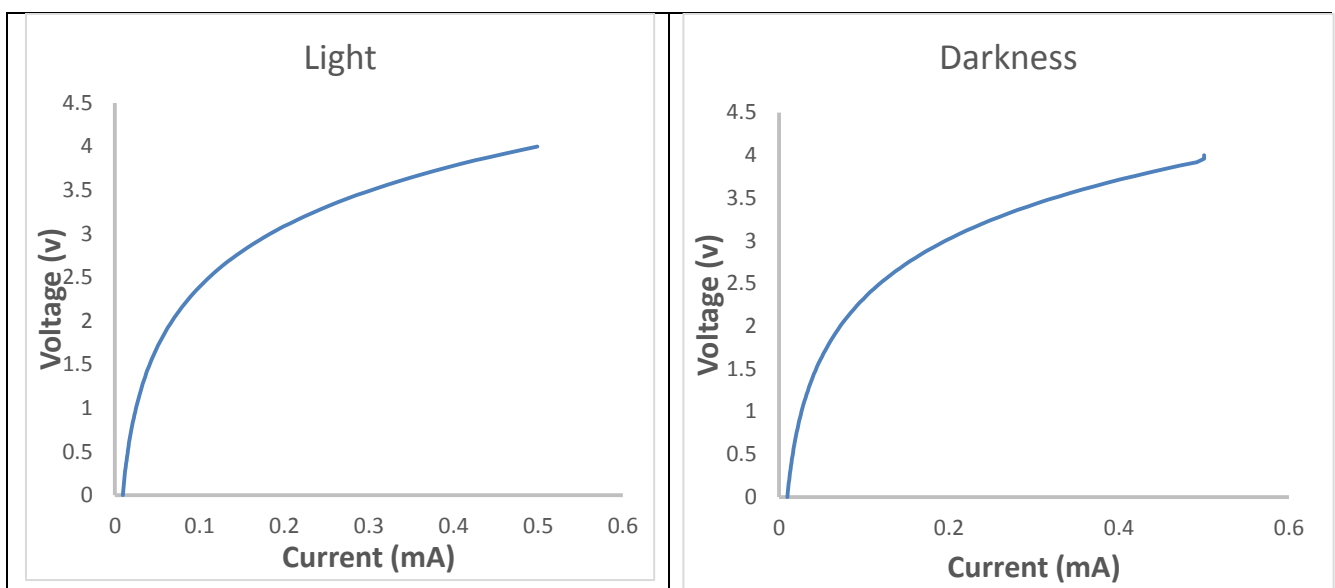


Figure (4-27) I-V test curve for 1000°C sample (BC3) at light and darkness

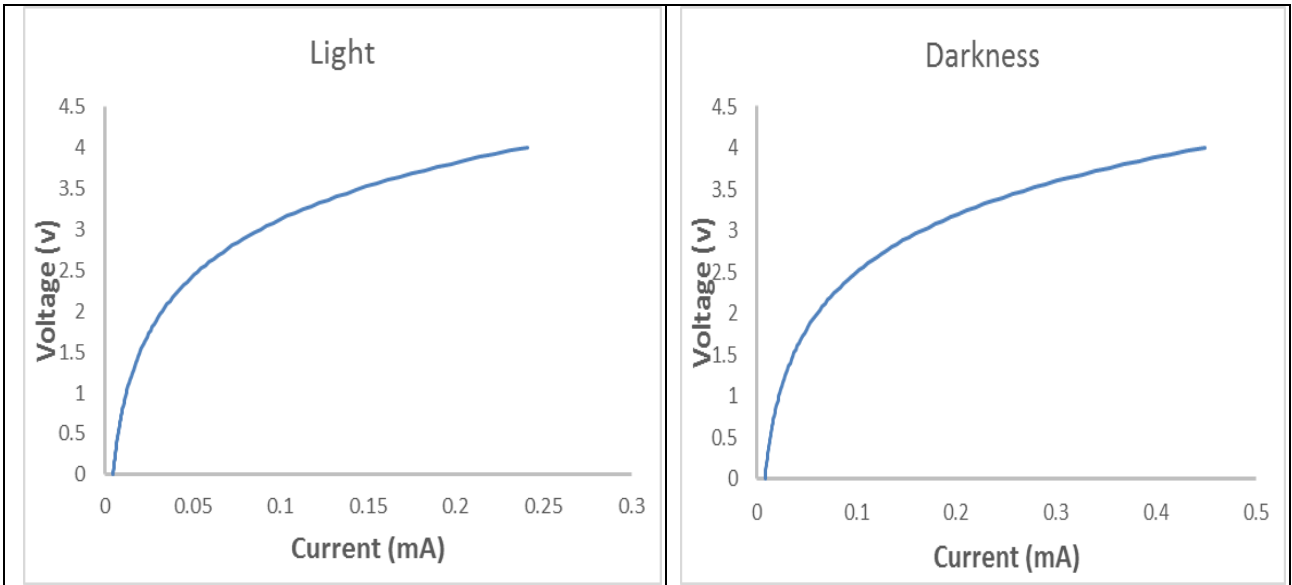


Figure (4-28) I-V test curve for 1050°C sample (BC3) at light and darkness

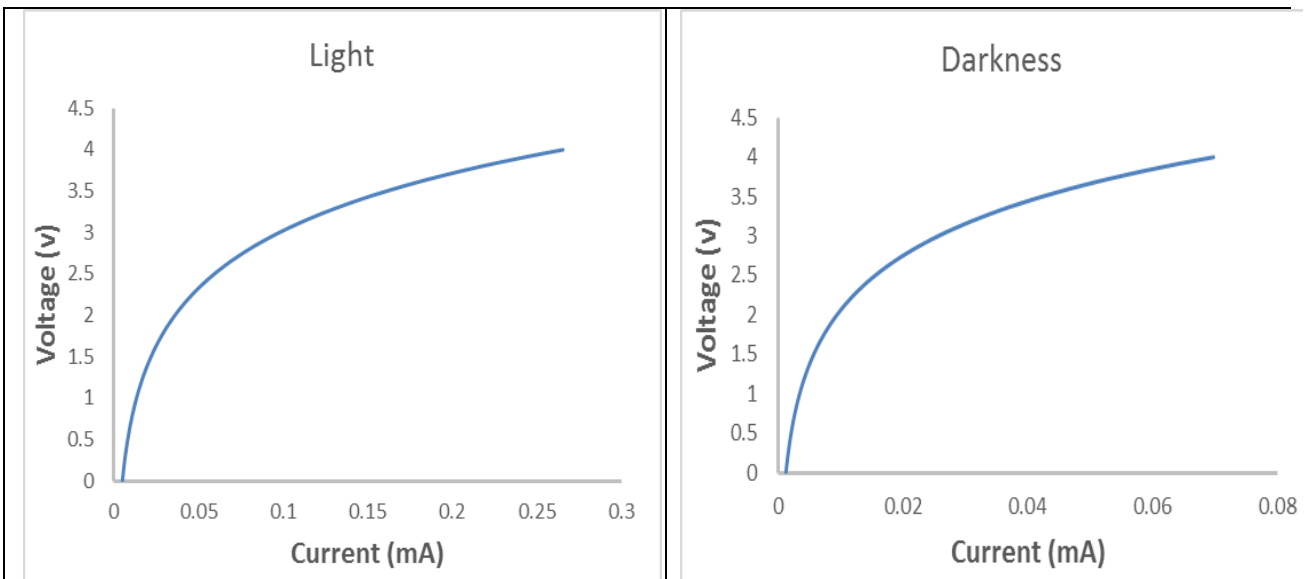


Figure (4-29) I-V test curve for 1100°C sample (BC3) at light and darkness

From the results obtained and shown in the figures above, it was found that the light intensity used on the samples did not significantly affect the I-V properties behavior as well as the presence of darkness. This enables us to take advantage of varistor in external conditions, including shining sunlight and within the safe area and operating outside the closed areas and exposing it to some nature conditions.

CHAPTER FIVE

CONCLUSION AND SUGGESTIONS

FOR FUTURE WORK

(5.1) Conclusion

We can conclude the following from the gained results.

- Zinc oxide used as an additive to many industrial materials including ceramics because of its good multiple characteristics, so it is used in varistor industry
- After mixing with certain metal oxides, zinc oxide behavior turned from linear to non-linear like (Bi_2O_3 , CoO , Sb_2O_3 , Cr_2O_3 and MnO_2), this will positively effect on the electrical properties of the varistor.
- The mixing of varistor with (In_2O_3) nano powder will inhibit grain growth and It increases the scale of improvement and improves the varistor microstructure thus improve its electrical properties such as (breakdown voltage, leakage current, Nonlinear coefficient and Dielectric properties).
- The elevated of sintering temperature has adversely affected on enlarge the grain size as well on the improvement of electrical properties of the varistor.
- After shedding the light intensity of tungsten on the varistor specimens for a fixed period of time, it shows that their electrical properties (I-V) characteristics are not affected. We are interested in taking advantage of the use of varistor in external environmental conditions.

(5.2) Future work

- Study the effect of mixing (In_2O_3) nano powder on mechanic features of Zinc oxide - based varistor.
- . Investigate of dopant (In_2O_3) nano powdon microstructure of SnO_2 based varistor
- Discuss the structure and electrical characteristics of ZnO-based varistor dopant with (In_2O_3) sintered less than (1000) °C with increase sintering time
- Increase the pressing process amount and pressing time to reduce porosity of ZnO varistor

REFERENCES

- 1.** Abdulsattar MA. Capped ZnO (3, 0) nanotubes as building blocks of bare and H passivated wurtzite ZnO nanocrystals. *Superlattices and Microstructures*. 2015 Sep 1;85:813-9.
- 2.** Hsu YW, Li HC, Yang YJ, Hsu CC. Deposition of zinc oxide thin films by an atmospheric pressure plasma jet. *Thin Solid Films*. 2011 Mar 1;519(10):3095-9.
- 3.** A. Khadim, “Electrical Properties & Microstructure Of ZnO - Based Varistor Ceramics Doped With Rare Earth,” University of Baghdad, 2015.
- 4.** Meshkatoddini MR. Metal oxide ZnO-based varistor ceramics. *Advances in Ceramics-Electric and Magnetic Ceramics, Bioceramics, Ceramics and Environment*. 2011 Sep 6.
- 5.** Levinson LM, Philipp HR. ZINC OXIDE VARISTORS- A REVIEW. *Am. Ceram. Soc. Bull.* 1986;65(4):639.
- 6.** Castleberry DE. Varistor-controlled liquid-crystal displays. *IEEE Transactions on Electron Devices*. 1979 Aug;26(8):1123-8.
- 7.** Nordlander J, Stefan DK, Yang P, Spoerke ED. The Effects of Calcination and Milling on Powder Characteristics and Electrical Behaviour of ZnO Varistor Materials. Sandia National Lab.(SNL-NM), Albuquerque, NM (United States); 2016 Dec 1.
- 8.** Yaya A, Dodoo-Arhin D. The influence of Bi_2O_3 and Sb_2O_3 doping on the microstructure and electrical properties of sintered zinc oxide. *ARPJ Journal of Engineering and Applied Sciences*. 2012;7:834-42.
- 9.** Furtado JG, Saléh LA, Serra ET, Oliveira GS, Nóbrega MC. Microstructural evaluation of rare-earth-zinc oxide-based varistor ceramics. *Materials Research*. 2005 Dec;8(4):425-9.

- 10.** Dosch RG, Tuttle BA, Brooks RA. Chemical preparation and properties of high-field zinc oxide varistors. *Journal of Materials Research*. 1986 Feb;1(1):90-9.
- 11.** Jiang F, Peng Z, Zang Y, Fu X. Progress on rare-earth doped ZnO-based varistor materials. *Journal of Advanced Ceramics*. 2013 Sep 1;2(3):201-12.
- 12.** Sedky A, El-Suheel E. A comparative study between the effects of magnetic and nonmagnetic dopants on the properties of ZnO varistors. *Physics Research International*. 2010 Apr 28;2010.
- 13.** Yang WZ, Zhou DL, Yin GF, Wang RS, Zhang Y. Characterization of ZnO based varistor derived from nano ZnO powders and ultrafine dopants. *JOURNAL OF MATERIALS SCIENCE & TECHNOLOGY*. 2005 Mar 1;21(2):183-6.
- 14.** Houabes M, Metz R. Rare earth oxides effects on both the threshold voltage and energy absorption capability of ZnO varistors. *Ceramics International*. 2007 Sep 1;33(7):1191-7.
- 15.** Janotti A, Van de Walle CG. Fundamentals of zinc oxide as a semiconductor. *Reports on progress in physics*. 2009 Oct 22;72(12):126501.
- 16.** Žunić M, Branković Z, Branković G. Electrical properties of ZnO varistors prepared by direct mixing of constituent phases. *Science of Sintering*. 2006;38(2):161-7.
- 17.** Dong XU, Shi XF, Cheng XN, Juan YA, Fan YE, Yuan HM, Shi LY. Microstructure and electrical properties of Lu₂O₃-doped ZnO-Bi₂O₃-based varistor ceramics. *Transactions of Nonferrous Metals Society of China*. 2010 Dec 1;20(12):2303-8.
- 18.** Chaari M, Matoussi A, Fakhfakh Z. Structural and dielectric properties of sintering zinc oxide bulk ceramic. *Materials Sciences and Applications*. 2011 Jul 20;2(07):764.

- 19.** Zhang CH, Li MS, Xu D, Chen YF, Liu YL, Zhang K. Microstructure and electrical properties of ZnO–Bi₂O₃-based varistor ceramics by different high-energy ball milling time. In *Advanced Materials Research 2012* (Vol. 490, pp. 3391-3395). Trans Tech Publications.
- 20.** Ji-le L, Chen GH, Yuan CL. Microstructure and electrical properties of rare earth doped ZnO-based varistor ceramics. *Ceramics International*. 2013 Apr 1;39(3):2231-7.
- 21.** Ke, L., Hu, M. and Ma, X., 2013. Preparation of Ultrahigh Potential Gradient of ZnO Varistors by Rare-Earth Doping and Low-Temperature Sintering. *Journal of Materials*, 2013
- 22.** Khafagy AM, El-Rabaie SM, Dawoud MT, Attia MT. Microhardness, microstructure and electrical properties of ZVM ceramics. *Journal of Advanced Ceramics*. 2014 Dec 1;3(4):287-96.
- 23.** A. F. Shannon, "The Effect of (Al₂O₃) Additive on Electrical Properties of (ZnO) - Based Varistor", University of Baghdad, 2016.
- 24.** Z. W. Ahmed, "Studying the Electrical Properties of Polymeric – Varistor Ceramic Composite", University of Baghdad, 2018.
- 25.** Sun Y, Wang H. The electronic properties of native interstitials in ZnO. *Physica B: Condensed Matter*. 2003 Jan 1;325:157-63.
- 26.** Rodnyi PA, Khodyuk IV. Optical and luminescence properties of zinc oxide. *Optics and Spectroscopy*. 2011 Nov 1;111(5):776-85.
- 27.** Morkoç H, Özgür Ü. Zinc oxide: fundamentals, materials and device technology. John Wiley & Sons; 2008 Dec 3.
- 28.** Mohamed Ehsan Hasan Ahmed, " A study of effected of Yttria stabilized Zirconia, addition on the mechanical and electrical properties of Zinc Oxide ceramic", Master thesis of Science in Physics , University of Baghdad- College of Education for pure science Ibn-Al-Haitham, 2011

- 29.** Zaman S. Synthesis of ZnO, CuO and their composite nanostructures for optoelectronics, sensing and catalytic applications (Doctoral dissertation, Linköping University Electronic Press).
- 30.** Erhart P, Albe K. Diffusion of zinc vacancies and interstitials in zinc oxide. Applied physics letters. 2006 May 15;88(20):201918.
- 31.** Dusan Galusek and Katrina Villanova. "Ceramic Material Classes", J. Ceramics Science and Technology, 2010.
- 32.** Jan Harloff , "In-situ quantitative measurement of electric fields in zinc oxide thin films using electrostatic force microscopy" ,A Master theses of Science , University of Pennsylvania , pp14-18 , 1995.
- 33.** Leite ER, Varela JA, Longo E. Barrier voltage deformation of ZnO varistors by current pulse. Journal of applied physics. 1992 Jul 1;72 (1) :147-50.
- 34.** Prof. A. D. Rollett , "Microstructure properties: the effect of grain size" , Scientific lectures, Carnegie Mellon University, (Lecture 6) ,pp.4-10, 20
- 35.** Elfwing M. Nanoscale characterisation of barriers to electron conduction in ZnO varistor materials (Doctoral dissertation, Acta Universitatis Upsaliensis).
- 36.** Bueno PR, Varela JA, Longo E. SnO₂, ZnO and related polycrystalline compound semiconductors: an overview and review on the voltage-dependent resistance (non-ohmic) feature. Journal of the European Ceramic Society. 2008 Jan 1;28(3):505-29.
- 37.** Hartmann Bálint, Ladányi József, Vokony István , "Electrical Systems Laboratory I. Theoretical Foundations of measurement", scientific research, Budapest University of Technology and Economics /Department of Electric Power Engineering,2004
- 38.** Lihui W, Guoyou G, Jialin S, Jikang Y. Preparation and characterization of layered low-voltage ZnO varistors. Journal of Semiconductors. 2009 Mar;30(3):033002.

- 39.** Lin C, Xu Z, Peng H. Densification and grain growth of microwave sintered ZnO varistors. *JOURNAL OF INORGANIC MATERIALS-BEIJING-*. 2007 Jan 1;22(5):917-21.
- 40.** Swarnakar AK, Donzel L, Vleugels J, Van der Biest O. High temperature properties of ZnO ceramics studied by the impulse excitation technique. *Journal of the European Ceramic Society*. 2009 Nov 1;29(14):2991-8.
- 41.** Begum S. Powder processing parameters and their influence on the electrical performance of ZnO varistor (Doctoral dissertation, Dublin City University).
- 42.** S. Mahata, "Preparation And Electrical Characterization Of Zinc Oxide Varistor", M.Sc thesis, Departement of instrumentation and electronics engineering, Jadavpur University Salt Lake Campus, 2010.
- 43.** Darvishi Alamdari H. Varistors prepared from nanocrystalline powders obtained by high-energy ball milling. 2001 Dec.
- 44.** Bueno PR, Varela JA, Longo E. SnO₂, ZnO and related polycrystalline compound semiconductors: an overview and review on the voltage-dependent resistance (non-ohmic) feature. *Journal of the European Ceramic Society*. 2008 Jan 1;28(3):505-29.
- 45.** Karim AN, Begum S. Enhanced Performance of Zinc Oxide Arrester by Simple Modification in Processing and Design. *J Material Sci Eng*. 2014;3(135):2169-0022.
- 46.** Pillai SC, Kelly JM, Ramesh R, McCormack DE. Advances in the synthesis of ZnO nanomaterials for varistor devices. *Journal of Materials Chemistry C*. 2013;1(20):3268-81.
- 47.** M. Hove, "Improvement Of The V-I Properties Of Zinc Oxide (ZnO) Based Metal Oxide Varistors(MOVs) Using Silicon Telluride (SiTe₂) And Lanthanum Hexaboride (LaB₆) Materials", Ph.D thesis, of Engineering and the Built Environment, University of Witwatersrand, 2006

48. Kelleher M. *Preparation of Metal Oxide Additive Particles Via Mechanical Methods and Their Influence on Subsequent Fabrication, Microstructural and Electrical Properties of Commercial ZnO Varistors* (Doctoral dissertation, Dublin City University. School of Mechanical and Manufacturing Engineering).

49. Pillai SC, Kelly JM, Ramesh R, McCormack DE. Advances in the synthesis of ZnO nanomaterials for varistor devices. *Journal of Materials Chemistry C*. 2013;1(20):3268-81.

50. Karim AN, Begum S. Enhanced Performance of Zinc Oxide Arrester by Simple Modification in Processing and Design. *J Material Sci Eng*. 2014;3(135):2169-0022.

51. Suresh V Vettoor, "Electrical conduction and superconductivity", physics research, physics department, St Dominic's college, Kanjirappally, pp.41-47, 2003.

52. Donald A. Neamen, "Semiconductor physics and devices – basic principles", third edition, ISBN 0-07-119862-8, p.104-107, 2003.

53. Bernik S, Podlogar M, Daneu N, Recnik A. Tailoring the microstructure of ZnO-based ceramics. *Materiali in tehnologije*. 2008 Mar 1;42(2):69.

54. Yoon JR, Lee CB, Lee KM, Lee HY, Lee SW. Voltage Enhancement of ZnO Oxide Varistors for Various Y₂O₃ Doping Compositions. *Transactions on Electrical and Electronic Materials*. 2009 Oct 25;10(5).

55. Suresh V Vettoor, "Electrical conduction and superconductivity", physics research, physics department, St Dominic's college, Kanjirappally, pp.41-47, 2003.

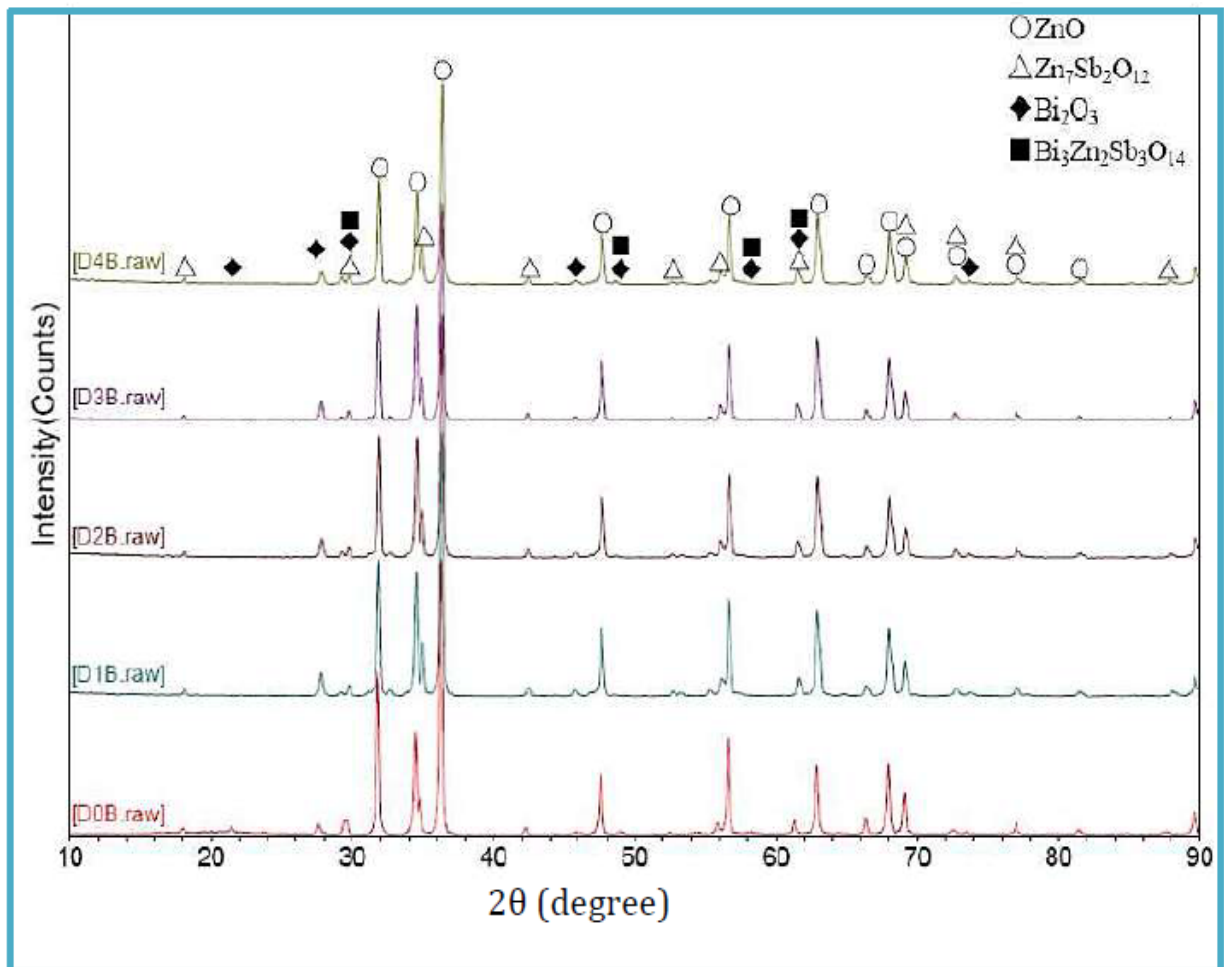
56. Nahm GW. Clamping Voltage Characteristics and Accelerated Aging Behavior of CoCrTb-doped Zn/Pr-based Varistors with Sintering Temperature. *Transactions on Electrical and Electronic Materials*. 2009;10(4):125-30.

- 57.** Tiwari A. Liquid phase sintering in microgravity. CURRENT SCIENCE-BANGALORE-. 2000 Aug 10;79(3):334-5.
- 58.** Vishnuvardhan TK, Kulkarni VR, Basavaraja C, Raghavendra SC. Synthesis, characterization and ac conductivity of polypyrrole/Y₂O₃ composites. Bulletin of Materials Science. 2006 Feb 1;29(1):77-83.
- 59.** Poonsuk Poosimma "Stability of zinc oxide varistor", PhD thesis in the faculty of engineering and physical sciences, School of materials-University of Manchester, PP. 16-36, 2014.
- 60.** Bernik S, Podlogar M, Daneu N, Rečnik A. A novel approach to tailoring the microstructure and electrical characteristics of ZnO-based varistor ceramics via inversion-boundary (IB) induced grain growth. Scientific paper UDC. 2011;620.
- 61.** Mahmood FS, Nadeem MY, Jamail U. A comprehensible need of zinc oxide varistors in electronics technology. Journal of Research (Science). 2007 Jul 15;18(3):185-95.
- 62.** Cramer CL. *Applications and advanced sintering techniques of functionally graded ZnO-based thermoelectric material* (Doctoral dissertation, Colorado State University. Libraries).
- 63.** Suk-Joong I. Kang " sintering Densification, Grain growth and Microstructure", ISBN: 978-0-7506-6385-4, P. 1-8, 2005.
- 64.** M. N. Rahaman, "Ceramic processing and sintering", Second edition, P. 425-625, 2003.
- 65.** Suk-Joong I. Kang " sintering Densification, Grain growth and Microstructure", ISBN: 978-0-7506-6385-4, P. 1-8, 2005.
- 66.** Docent. N. Menad, "Sintering and consolidation of ceramics" , Lectures series, Dept. of Chemical engineering – Lulea University of technology (Sweden), Course, KGP003, 2003.
- 67.** Lutgard C. DE Jonghe and Mohamed N. Rahaman, "Sintering of ceramics Handbook of advance ceramics", pp.187-189, 2003

68. Lavina B, Dera P, Downs RT. Modern X-ray diffraction methods in mineralogy and geosciences. *Reviews in Mineralogy and Geochemistry*. 2014 Jan 1;78(1):1-31.
69. Lavina B, Dera P, Downs RT. Modern X-ray diffraction methods in mineralogy and geosciences. *Reviews in Mineralogy and Geochemistry*. 2014 Jan 1;78(1):1-31.
70. Theivasanthi T, Alagar M. X-ray diffraction studies of copper nanopowder. arXiv preprint arXiv:1003.6068. 2010 Mar 31.
71. Le Bail A. Powder diffraction: theory and practice. Royal Society of Chemistry; 2008.
72. Dang Anh Tuan, Vo Thanh Tung, Le Van Phuong, "Analyzing 2D structure images of piezoelectric ceramics using image J", *Intern. J. of material and ceramics*, vol.4, No.4, PP.88-91, 2014.
73. Muayad J. Yusif " Solid state physics– part one", second edition,PP.138, 1987.
74. Zang GZ, Wang JF, Chen HC, Su WB, Wang WX, Wang CM, Qi P. Effect of In₂O₃ doping and sintering on the electrical properties and the microstructure of (Co, Ta)-doped SnO₂ varistors. *Journal of non-crystalline solids*. 2005 Apr 15;351(10-11):941-5.
75. Fernandez-Hevia D, Peiteado M, De Frutos J, Caballero AC, Fernandez JF. Wide range dielectric spectroscopy of ZnO-based varistors as a function of sintering time. *Journal of the European Ceramic Society*. 2004 Jan 1;24(6):1205-8.
76. Fernandez-Hevia D, Peiteado M, De Frutos J, Caballero AC, Fernandez JF. Wide range dielectric spectroscopy of ZnO-based varistors as a function of sintering time. *Journal of the European Ceramic Society*. 2004 Jan 1;24(6):1205-8.

77. KANG X, SONG S, HAN Y, TU M, TAO M. INFLUENCE OF ZnO NANOMETER POWDERS ON MICROSTRUCTURE AND ELECTRICAL PROPERTIES OF VARISTOR MATERIAL [J]. CHINESE JOURNAL OF MATERIAL RESEARCH. 1996;5.

78. Nahm CW. Effect of aluminum addition on electrical properties, dielectric characteristics, and its stability of (Pr, Co, Cr, Y)-added zinc oxide-based varistors. Bulletin of Materials Science. 2010 Jun 1;33(3):239-45.



XRD patterns of (ZnO-Bi₂O₃) varistor at five different milling time [23]

00-006-0416 (Fixed Slit Intensity) - Cu Ka1 1.54056Å

| 2θ | d(Å) | I | h | k | l | * | 2θ | d(Å) | I | h | k | l | * | 2θ | d(Å) | I | h | k | l | * | |
|---------|-----------------|-----|---|---|---|---|---------|----------|----|---|---|---|---|---------|----------|----|---|---|---|---|--|
| 17.5123 | 5.060000 | 1 | 2 | 0 | 0 | E | 55.9903 | 1.641000 | 6 | 6 | 1 | 1 | | 79.1550 | 1.209000 | 4 | 6 | 5 | 3 | | |
| 21.4982 | 4.130000 | 14 | 2 | 1 | 1 | | 57.5570 | 1.600000 | 2 | 6 | 2 | 0 | | 80.5126 | 1.192000 | 2 | 8 | 2 | 2 | | |
| 30.5799 | 2.921000 | 100 | 2 | 2 | 2 | | 59.1356 | 1.561000 | 4 | 5 | 4 | 1 | | 81.8224 | 1.176200 | 4 | 8 | 3 | 1 | | |
| 33.1018 | 2.704000 | 2 | 3 | 2 | 1 | | 60.6762 | 1.525000 | 25 | 6 | 2 | 2 | | 83.1640 | 1.160600 | 6 | 6 | 6 | 2 | | |
| 35.4657 | 2.529000 | 30 | 4 | 0 | 0 | | 62.1652 | 1.492000 | 6 | 6 | 3 | 1 | | 84.5022 | 1.145600 | <1 | 7 | 5 | 2 | | |
| 37.6851 | 2.385000 | 8 | 4 | 1 | 1 | | 63.6854 | 1.460000 | 6 | 4 | 4 | 4 | | 85.8344 | 1.131200 | 4 | 8 | 4 | 0 | | |
| 39.8184 | 2.262000 | 2 | 4 | 2 | 0 | | 65.1334 | 1.431000 | 2 | 5 | 4 | 3 | | 87.1672 | 1.117300 | 2 | 8 | 3 | 3 | | |
| 41.8453 | 2.157000 | 6 | 3 | 3 | 2 | | 66.6001 | 1.403000 | 2 | 6 | 4 | 0 | | 88.4883 | 1.104000 | 2 | 8 | 4 | 2 | | |
| 43.7813 | 2.066000 | 2 | 4 | 2 | 2 | | 68.0272 | 1.377000 | 4 | 7 | 2 | 1 | | 89.8154 | 1.091100 | 2 | 7 | 6 | 1 | | |
| 45.6908 | 1.984000 | 10 | 4 | 3 | 1 | | 69.4633 | 1.352000 | 2 | 6 | 4 | 2 | | 91.1468 | 1.078600 | <1 | 6 | 6 | 4 | | |
| 49.2677 | 1.848000 | 4 | 5 | 2 | 1 | | 73.6596 | 1.285000 | 4 | 6 | 5 | 1 | | 92.4812 | 1.066500 | 2 | 8 | 5 | 1 | | |
| 51.0374 | 1.788000 | 35 | 4 | 4 | 0 | | 75.0225 | 1.265000 | 4 | 8 | 0 | 0 | | 95.1394 | 1.043600 | 2 | 9 | 3 | 2 | | |
| 52.7143 | 1.735000 | 4 | 4 | 3 | 3 | | 76.3699 | 1.246000 | 4 | 7 | 4 | 1 | | 96.4711 | 1.032700 | 4 | 8 | 4 | 4 | | |
| 54.3704 | 1.686000 | 2 | 6 | 0 | 0 | | 77.7723 | 1.227000 | 2 | 8 | 2 | 0 | | | | | | | | | |

Pdf for Xrd card for In2O3 powder

00-036-1461 (Fixed Slit Intensity) - Cu Ka1 1.54056Å

| 2θ | d(Å) | I | h | k | l | * | 2θ | d(Å) | I | h | k | l | * | 2θ | d(Å) | I | h | k | l | * | |
|---------|-----------------|-----|---|---|---|---|---------|----------|----|---|---|---|---|---------|----------|----|---|---|---|---|--|
| 16.4616 | 5.380520 | 2 | 1 | 1 | 0 | | 45.9687 | 1.972650 | 24 | 0 | 4 | 1 | | 65.2584 | 1.428560 | 8 | 4 | 3 | 1 | | |
| 20.8025 | 4.266520 | 50 | 1 | 0 | 1 | | 47.6988 | 1.905060 | 5 | 2 | 2 | 2 | | 65.6014 | 1.421920 | <1 | 3 | 0 | 3 | | |
| 20.9445 | 4.237920 | 51 | 0 | 2 | 0 | | 48.3938 | 1.879310 | 8 | 1 | 3 | 2 | | 66.1062 | 1.412280 | <1 | 0 | 6 | 0 | | |
| 23.3244 | 3.810600 | 40 | 1 | 1 | 1 | | 50.8906 | 1.792810 | 19 | 3 | 3 | 0 | | 66.4390 | 1.406010 | 3 | 1 | 5 | 2 | | |
| 24.5694 | 3.620260 | 15 | 1 | 2 | 0 | | 52.4827 | 1.742110 | 8 | 1 | 0 | 3 | | 66.6543 | 1.401990 | 15 | 3 | 1 | 3 | | |
| 25.5794 | 3.479560 | 22 | 2 | 0 | 0 | | 53.1237 | 1.722590 | 2 | 3 | 1 | 2 | | 67.2452 | 1.391100 | 8 | 2 | 3 | 3 | | |
| 26.7124 | 3.334490 | 67 | 0 | 2 | 1 | | 53.3395 | 1.716130 | 4 | 2 | 4 | 1 | | 67.6083 | 1.384510 | 4 | 1 | 6 | 0 | | |
| 27.6893 | 3.219020 | 53 | 2 | 1 | 0 | | 53.7465 | 1.704090 | 19 | 4 | 1 | 0 | | 67.7599 | 1.381780 | 2 | 4 | 2 | 2 | | |
| 29.6793 | 3.007560 | 88 | 1 | 2 | 1 | | 53.8424 | 1.701280 | 16 | 3 | 3 | 1 | | 68.3280 | 1.371670 | 8 | 0 | 4 | 3 | | |
| 32.3512 | 2.765000 | 40 | 2 | 1 | 1 | | 55.4316 | 1.656210 | 9 | 0 | 2 | 3 | | 68.4963 | 1.368710 | 14 | 3 | 5 | 0 | | |
| 33.1541 | 2.699850 | 43 | 0 | 0 | 2 | | 55.7615 | 1.647190 | 4 | 1 | 5 | 0 | | 68.6151 | 1.366630 | <1 | 0 | 6 | 1 | | |
| 34.2112 | 2.618810 | 10 | 1 | 3 | 0 | | 56.5875 | 1.625090 | 7 | 4 | 1 | 1 | | 69.6070 | 1.349560 | 8 | 0 | 0 | 4 | | |
| 37.2300 | 2.413100 | 5 | 1 | 1 | 2 | | 56.7436 | 1.620990 | 22 | 1 | 4 | 2 | | 69.7442 | 1.347240 | 7 | 5 | 0 | 1 | | |
| 37.3140 | 2.407860 | 20 | 2 | 2 | 1 | | 57.1153 | 1.611320 | 12 | 1 | 2 | 3 | | 70.1151 | 1.341020 | 8 | 1 | 6 | 1 | | |
| 38.1720 | 2.355690 | 2 | 1 | 3 | 1 | | 58.5475 | 1.575270 | 2 | 1 | 5 | 1 | | 70.7429 | 1.330650 | 2 | 5 | 1 | 1 | | |
| 39.5489 | 2.276790 | 20 | 0 | 2 | 2 | | 58.7505 | 1.570310 | 7 | 2 | 1 | 3 | | 70.9878 | 1.326660 | 3 | 3 | 5 | 1 | | |
| 40.2750 | 2.237400 | 5 | 3 | 1 | 0 | | 59.9365 | 1.542040 | 1 | 4 | 2 | 1 | | 71.2730 | 1.322050 | 3 | 5 | 2 | 0 | | |
| 41.1140 | 2.193660 | 7 | 2 | 3 | 0 | | 60.7193 | 1.524020 | 1 | 2 | 5 | 0 | | 72.3878 | 1.304410 | 3 | 4 | 4 | 1 | | |
| 41.7088 | 2.163740 | 30 | 1 | 2 | 2 | | 62.1102 | 1.493190 | 23 | 3 | 3 | 2 | | 73.5982 | 1.285920 | 6 | 0 | 2 | 4 | | |
| 42.3428 | 2.132800 | 7 | 2 | 0 | 2 | | 62.6061 | 1.482550 | 1 | 1 | 3 | 3 | | 73.7271 | 1.283990 | 3 | 5 | 2 | 1 | | |
| 43.7479 | 2.067500 | 100 | 2 | 1 | 2 | | 63.3611 | 1.466690 | 8 | 2 | 5 | 1 | | 74.2837 | 1.275740 | 1 | 2 | 4 | 3 | | |
| 44.5449 | 2.032340 | 58 | 2 | 3 | 1 | | 63.5881 | 1.462000 | 7 | 4 | 0 | 2 | | | | | | | | | |
| 44.6639 | 2.027200 | 54 | 1 | 4 | 0 | | 64.6503 | 1.440520 | 12 | 4 | 1 | 2 | | | | | | | | | |

Pdf for Xrd card for pure ZnO powder

الخلاصة:

الفارستور هو جهاز مصنوع من مواد سيراميكية. يتم استخدامه كعنصر حماية في العديد من مجالات الحياة. ومن اجل تحضير الفارستور تستخدم الطريقة التقليدية لصناعات السيراميك (تفاعل الحالة الصلبة).

تم اجراء اختبارات الاشعة السينية لمسحوق اوكسيد الزنك ومسحوق اوكسيد الانديوم النانوي لتحديد درجة النقاوة. بعد عملية الوزن ، تم خلط المساحيق بالماء بواسطة خلاط مغناطيسي ثم تجفيفها لمدة 24 ساعة. بعد ذلك ، يتم التخلص من الغازات والرطوبة وبعض من الشوائب عن طريق الحرق لمدة 2 ساعة في (500 درجة مئوية). ثم يتم إجراء الطحن ، ويتم ضغط العينات في أقراص نصف قطرها 8 مم. توضع العينات في الفرن للتليد عند ثلاث درجات حرارة مختلفة (1000 ، 1050 و 1100) درجة مئوية للحصول على الأشكال المطلوبة.

تم اجراء فحوصات الاشعة السينية للعينات الملبدة وتبين ظهور عدة اطوار والتي كان على رأسها طور اوكسيد الزنك الاساسي. تم قياس حجم البلورات وحجم الحبوب من العينات باستخدام معادلة ديبي-شيرر وصور المجهر الإلكتروني المسح واتضح أن حجم الحبوب ينقص بزيادة تركيز مسحوق اوكسيد الانديوم النانوي ويزيد مع زيادة درجة حرارة التليد.

لأن تأثير انهيار الجهد على حجم الحبوب ، فإنه سيزيد بزيادة تركيز مسحوق أوكسيد الإنديوم النانوي . يمكن رؤية سلوك المعامل غير الخطي (α) بين قيم التيار والجهد. لقد وجد أن المعامل غير الخطي يزداد بزيادة تركيز مسحوق (In_2O_3) النانوي وأكاسيد أخرى. يعود سبب انخفاض (α) مع زيادة درجات حرارة التليد إلى تأثير حواجز شوتكي بين حدود الحبوب. علاوة على ذلك ، عند ارتفاع درجة الحرارة انخفض تيار التسرب عند زيادة تراكيز مسحوق (In_2O_3) النانوي.

تم تخفيض قيم ثابت العزل عن طريق زيادة التردد ويلاحظ ارتفاع ثابت العزل الكهربائي مع ارتفاع درجات الحرارة التليد. ومع ذلك ، فإن نتائج عامل الخسارة تتناقص مع زيادة تراكيز اوكسيد الانديوم النانوي.

تم فحص تأثير الضوء والظلام على خصائص (تيار-الفولتية) للعينات بعد تسليط شدة الضوء عليها وكذلك في العتمة. تبين أن الخصائص الكهربائية للعينات لا تتأثر بكلا الاختبارين ، مما يسمح لنا بالاستفادة من استخدام الفارستور في الظروف البيئية الخارجية ، وخاصة تأثير ضوء الشمس.



جمهورية العراق

وزارة التعليم العالي والبحث العلمي

جامعة بغداد

كلية التربية للعلوم الصرفة (ابن الهيثم)

تأثير أوكسيد الانديوم على الخصائص الكهربائية لفارستور أوكسيد الخارصين

رسالة قدمها

مصطفى قاسم عباس

إلى

مجلس كلية التربية للعلوم الصرفة (ابن الهيثم) - جامعة

بغداد

كجزء من متطلبات نيل درجة الماجستير في الفيزياء

بإشراف

أ.م. د. أيسر جمعة إبراهيم

2019 م

1441 هـ